
ReinFlow: Fine-tuning Flow Matching Policy with Online Reinforcement Learning

Tonghe Zhang

Robotics Institute
School of Computer Science
Carnegie Mellon University
tonghez@andrew.cmu.edu

Chao Yu*

Department of Electronic Engineering
Tsinghua University
Beijing Zhongguancun Academy
zoeyuchao@gmail.com

Sichang Su

Department of Aerospace Engineering
The University of Texas at Austin
sichang_su@utexas.edu

Yu Wang

Department of Electronic Engineering
Tsinghua University
yu-wang@mail.tsinghua.edu.cn

Abstract

We propose ReinFlow, a simple yet effective online reinforcement learning (RL) framework that fine-tunes a family of flow matching policies for continuous robotic control. Derived from rigorous RL theory, ReinFlow injects learnable noise into a flow policy’s deterministic path, converting the flow into a discrete-time Markov Process for exact and straightforward likelihood computation. This conversion facilitates exploration and ensures training stability, enabling ReinFlow to fine-tune diverse flow model variants stably, including Rectified Flow [34] and Shortcut Models [18], particularly at very few or even one denoising step. We benchmark ReinFlow in representative locomotion and manipulation tasks, including long-horizon planning with visual input and sparse reward. The episode reward of Rectified Flow policies obtained an average net growth of 135.36% after fine-tuning in challenging legged locomotion tasks while saving denoising steps and 82.63% of wall time compared to state-of-the-art diffusion RL fine-tuning method DPPO [42]. The success rate of the Shortcut Model policies in state and visual manipulation tasks achieved an average net increase of 40.34% after fine-tuning with ReinFlow at four or even one denoising step, whose performance is comparable to fine-tuned DDIM policies while saving computation time for an average of 23.20%. Code, model, and checkpoints available on the project website: <https://reinflow.github.io/>

1 Introduction

Recent years have seen rapid progress in the training of robotic models via imitation learning. Flow matching models, which combine the trifecta of precise modeling, fast inference, and minimal implementation, have emerged as a robust alternative to diffusion policies and a popular choice for robot action generation [8, 6, 57].

However, due to the scarcity of robot data and the embodiment gap, flow policies and many other imitation learning policies are often trained from datasets with mixed quality [13], incurring suboptimal success rates even after supervised fine-tuning [6]. Although collecting more data may alleviate this problem, recent work [31] suggests that scaling the quantity of data may not be a panacea because, in a given environment, the success rate quickly plateaus when we only increase the number of

*Corresponding author

demonstrations. Worse still, as an imitation learning method, flow policies lack a built-in exploration mechanism, implying that robots trained on imperfect data could struggle to complete challenging tasks where the agent needs to surpass expert demonstrations [5].

Online reinforcement learning (RL) offers a promising solution to these challenges. By learning through trial and error, RL promises to overcome limitations associated with imperfect expert data and even achieve superhuman performance. Although recent studies have shown that it is possible to fine-tune diffusion policies via RL [30, 42], training flow models with online RL remains technically challenging.

First, the theory has established that the refinement of a stochastic policy is vital for continuous control problems [49]. However, for conditional flows, whose sample path is governed by a neural ordinary differential equation (ODE), even the log probability—a key factor that measures this stochasticity—could be challenging to obtain and unstable to backpropagate through. This problem is exacerbated when we infer flow policies at very few denoising steps, where the discretization error becomes large at a low inference cost. Second, compared to offline RL methods, online RL fine-tuning requires the policy to balance exploration and exploitation, especially in sparse reward settings [20]. However, how to design a principled exploration mechanism remains elusive for conditional flows with a deterministic path.

This paper addresses these challenges head-on and proposes the first online RL approach to fine-tune a pre-trained flow matching policy. The contributions of this work are summarized as follows:

- *Algorithm Design.* We propose ReinFlow, the first online RL algorithm to stably fine-tune a family of flow matching policies, especially in very few or even in one denoising step. We train a noise injection network to convert flows to a discrete-time Markov process with Gaussian transition probabilities for exact and tractable likelihood computation. Our design allows the noise net to automatically balance exploration with exploitation; it enjoys lightweight implementation, built-in exploration, and broad applicability to various variants of flow policy, including those parameterized with Rectified Flow [34] and Shortcut Models [18].
- *Empirical Validation.* We perform extensive experiments in representative robot locomotion and manipulation tasks, with the agent receiving state or pixel observations and possibly accepting sparse rewards. Without reward shaping or scaling off-line data, our method, on average, improves the success rate over the pre-trained manipulation policy by 40.34% and increases the reward of locomotion policies by 135.36%. We achieve this improvement with a wall time reduction of 62.82% for all tasks compared to the state-of-the-art diffusion RL method DPPO [42].
- *Scientific Understanding.* We carry out systematic sensitivity analysis on design choices and key factors affecting the performance of our method, ReinFlow, including the scale of pretrained data, the number of denoising steps, the conditioning of the noise network, the level of noise and the type and intensity of different regularizations.

2 Related Work

In this section, we provide an outline of the relevant work. We defer a detailed introduction for several key baselines to the Appendix B.

Online RL for improving diffusion-based policies. Training diffusion-based policies from demonstrations has recently achieved impressive results in a variety of robot learning tasks [3, 12, 39, 43, 50, 53, 56]. However, their performance remains highly dependent on the quality of the demonstration data. In practice, demonstrations often contain mixed or suboptimal trajectories, which limits policy effectiveness and motivates the need for online fine-tuning.

Several offline diffusion-based RL methods can be extended to online settings. For example, Diffusion Q-Learning (DQL) [54] and Implicit Diffusion Q-Learning (IDQL) [23] treat diffusion models as stochastic action policies and apply Q-learning updates. DIPO [55] adopts a similar idea, but employs a critic to directly refine the actions sampled using action gradients. Although these approaches leverage Q-function approximations to guide the diffusion actor, inaccurate Q estimates can introduce bias and destabilize training.

Alternatively, methods such as Q-Score Matching (QSM) [41] and Diffusion Policy Policy Optimization (DPPO) [42] fine-tune pre-trained diffusion policies using policy gradient techniques. Despite the growing interest in online RL for diffusion-based policies, by the time we release this work, few analogous methods exist for flow-based policies. The underlying mathematical distinctions between diffusion and flow models prevent direct adaptation of existing techniques [33], which poses additional challenges to develop effective online RL algorithms for flow policies.

Reinforcement Learning for Flow Matching Models. Flow matching models are more efficient than diffusion models, offering faster training, sampling, and better generalization [32, 58]. Following their success in imitation learning [8, 57] and vision tasks [32, 16, 27, 52], recent work has begun integrating them into reinforcement learning (RL).

Flow Q-Learning (FQL) [38] trains flow policies offline and distills them for fine-tuning but lacks exploration during online adaptation, leading to suboptimal convergence. ReinFlow addresses this by injecting bounded, learnable noise into flow trajectories to promote exploration.

While Flow-GRPO [33] and ORW-CFM-W2 [17] also study online RL for flow models, they focus on vision tasks rather than continuous robotic control. ReinFlow instead provides a general policy gradient framework with a compact noise network and exact likelihood computation, unlike Flow-GRPO’s fixed noise or ORW-CFM-W2’s reward-weighted regression approach.

3 Problem Formulation

Robot Learning as a Decision Process We formulate robot learning as an infinite-horizon Partially Observable Markov Decision Process (POMDP) in continuous state space $\mathcal{S} \in \mathbb{R}^{d_S}$, action space $\mathcal{A} \in \mathbb{R}^{d_A}$, observation space $\mathcal{O} \in \mathbb{R}^{d_O}$, with a reward discount factor $\gamma \in (0, 1)$. The robot plays in an environment with an unknown transition kernel $\mathbb{T}_{h,a}(\cdot|s)$ and an emission kernel $\mathbb{O}_h(\cdot|s)$. The interactions start with an initial state S_0 drawn from a distribution $\rho \in \mathcal{D}(\mathcal{S})$. In step $h \in \mathbb{Z}_{\geq 0}$, agent observes $o_h \sim \mathbb{O}_h(\cdot|s_h)$, takes an action a_h , before the state s_h transitions to $s_{h+1} \sim \mathbb{T}_{h,a_h}(\cdot|s_h)$ with reward r_h . For simplicity, we study reactive policies, which map the latest observation to an action distribution. The agent aims to maximize the discounted accumulated reward $J(\pi) = \mathbb{E}^\pi \left[\sum_{h=0}^{+\infty} \gamma^h r_h(a_h, o_h) \right]$. The Q function value function and the advantage function are defined as

$$Q_h^\pi(o_h, a_h) := \mathbb{E}^\pi \left[\sum_{\tau=h}^{+\infty} \gamma^{\tau-h} r_\tau \mid o_h, a_h \right], \quad V_h^\pi(o_h) = \mathbb{E}^\pi [Q_h^\pi(o_h, a_h) | o_h], \quad A_h^\pi := Q_h^\pi - V_h^\pi \quad (1)$$

We drop the subscript h for V_h^π , Q_h^π , and A_h^π when the policy and POMDP are stationary.

Flow Matching Models Flow matching [32] transforms random variables from one distribution p_0 to another p_1 with flow mappings $\psi : [0, 1] \times \mathcal{X} \rightarrow \mathcal{X}$, where $X_t := \psi_t(X_0)$, $t \in [0, 1]$. This process is associated with an ODE: $\frac{d}{dt} \psi_t(X_0) = v(t, \psi_t(X_0))$ where $X_0 \sim p_0$. Rectified flow (ReFlow) [34]² is a simple flow model with a straight ODE path $X_t = tX_1 + (1-t)X_0$. The velocity field for Rectified Flow satisfies $v(t, X_t) = \frac{d}{dt} X_t = X_1 - X_0$, which implies that the training objective for Rectified Flow is given by

$$\hat{\theta} = \arg \min_{\theta} \mathbb{E}_{X_0 \sim p_0, X_1 \sim p_1, t \sim \text{Unif}[0,1]} \left[\|X_1 - X_0 - v_\theta(t, X_t)\|_2^2 \right] \quad (2)$$

Practitioners also sample t from the beta distribution [7] or the logit normal distribution [16]. [18] proposes “Shortcut Models” to further improve the generation quality of Rectified Flow at very few denoising steps by enforcing the velocity generated by two steps to align with that generated by a single step. During inference, we numerically solve the transport equation by integrating the learned velocity field: $\dot{X}_1 = X_0 + \sum_{k=0}^{K-1} v_\theta(t_i, X_{t_i}) \Delta t_i$, where K is the number of denoising steps, $0 = t_0 < t_1 < \dots < t_{K-1} < 1 = t_K$ are the discretized time steps, $\Delta t_i = t_{i+1} - t_i$ is the step size.

Flow Matching Policy When we instantiate a flow-matching model in the action-generation setting, we obtain a flow-matching policy for robot learning. We denote by a_h^t the denoised action at time t

²For simplicity, we only consider 1-ReFlow and use 1-ReFlow and ReFlow in this work interchangeably.

generated during the h -th step of the episode. \mathcal{X} will be the action space \mathcal{A} , p_0 will be the standard normal distribution, and X_t corresponds to the robot’s denoised actions. The velocity field v_θ also conditions the observations.

Flow policies offer significantly faster inference than autoregressive and diffusion models [7, 57]. A fast policy is valuable for robot learning, as a high inference frequency enhances the robot’s dexterity, and faster rollouts also reduce the wall-clock time of RL fine-tuning. Reducing denoising steps is arguably the most straightforward method to further accelerate flow policies, but when numerically solving the ODE, fewer integration steps increase the discretization error and reduce the quality of action generation [45]. This work seeks to use RL to improve flow policies with minimal denoising steps, ideally a single step, to achieve the best of both worlds: rapid inference and high success rates.

4 Algorithm Design

In this section, we detail the design of our algorithm “ReinFlow”. We begin in Section 4.1 by introducing a methodology that precisely computes the logarithmic probability of the action in a simple closed form. This approach leverages the injection of Markov noise and eliminates the discretization error, making it applicable even with minimal denoising steps. Next, in Section 4.2, we derive a general policy gradient loss for arbitrary policies parameterized by a discrete-time Markov process, and then specialize this result in our noise-injected flow policy. Following this, Sections 4.3 and 4.4 detail the design choices for the noise injection network and the regularization techniques employed to enhance stability and promote exploration.

Algorithm 1 ReinFlow

- 1: **Input** pre-trained flow matching policy’s velocity field v_θ ; denoising step number K , discount factor γ , batch size B , discretization scheme $0 = t_0 < t_1 < \dots < t_K = 1$ with $\Delta t_k := t_{k+1} - t_k$ regularization function \mathcal{R} with intensity coefficient $\alpha \in \mathbb{R}$.
 - 2: **Initialize** noise injection network θ' .
 - 3: **while** not converged **do**
 - 4: Restore last iteration’s parameters: $\bar{\theta}_{\text{old}} \leftarrow \text{stop_grad}([\theta, \theta'])$
 - 5: **Reset** environment and receive initial observation o .
 - 6: **while** not done **do** ▷ Rollout policy π .
 - 7: Sample $a^0 \sim \mathcal{N}(0, \mathbb{I}_{d_A})$
 - 8: **for** denoising step k in $\{0, 1, \dots, K-1\}$ **do** ▷ Inject noise and integrate.
 - 9: $a^{k+1} \leftarrow a^k + v_\theta(t_k, a^k, o) \Delta t_k + \sigma_{\theta'}(t_k, a^k, o) \epsilon, \quad \epsilon \sim \mathcal{N}(0, \mathbb{I}_{d_A})$
 - 10: **end for**
 - 11: Record denoised actions a^0, a^1, \dots, a^K in a buffer.
 - 12: Play action $a = a^K$, receive reward r and done flag d , update observation o .
 - 13: Store $\{\mathbf{a}, o, r, d\}$ to buffer, where $\mathbf{a} := (a^0, a^1, \dots, a^K)$
 - 14: **end while**
 - 15: Sample a batch of data $\{\mathbf{a}_i, o_i, r_i, d_i\}_{i=1}^B$ from buffer. ▷ Optimize policy.
 - 16: Compute the policy’s transition probability for each denoising step k by Eq. (7):
 - 17:
$$\ln \pi^{\bar{\theta}}(a_i^{k+1} | a_i^k, o_i) = \ln \mathcal{N}(a_i^{k+1} | a_i^k + v_\theta(t_k, a_i^k, o_i) \Delta t_k, \sigma_{\theta'}^2(t_k, a_i^k, o_i))$$
 - 18: Compute the regularization function \mathcal{R} evaluated on each tuple, denoted as $\mathcal{R}(\mathbf{a}_i, o_i; \bar{\theta}, \bar{\theta}_{\text{old}})$.
 - 19: Call a policy gradient sub-routine, such as Alg. 2, to jointly optimize θ and θ' by Eq. (9):
 - 20:
$$\theta, \theta' = \underset{\theta, \theta'}{\operatorname{argmin}} \frac{1}{B} \sum_{i=1}^B \left[-A^{\bar{\theta}_{\text{old}}}(o_i, a_i) \sum_{k=0}^{K-1} \ln \pi^{\bar{\theta}}(a_i^{k+1} | a_i^k, o_i) + \alpha \cdot \mathcal{R}(\mathbf{a}_i, o_i; \bar{\theta}, \bar{\theta}_{\text{old}}) \right] \quad (3)$$
 - 21: where $\bar{\theta} := [\theta, \theta']$
 - 20: **end while**
 - 21: **Return** fine-tuned flow matching policy’s velocity field v_θ .
-

Algorithm 2 ReinFlow Subroutine for Policy Optimization (PPO implementation)

- 1: **Input** clipping range $\epsilon \in (0, 1)$, policy parameters at the current iteration $\bar{\theta} := [\theta, \theta']$ and the last iteration θ_{old} , data $\{\mathbf{a}_i, o_i, r_i, d_i\}_{i=1}^B$, regularization function values $\{\mathcal{R}(\mathbf{a}_i, o_i; \bar{\theta}, \theta_{\text{old}})\}_{i=1}^B$, with intensity $\alpha \in \mathbb{R}$.
- 2: Compute the advantage estimates $\hat{A}_i := \hat{A}(o_i, a_i^K)$ by methods such as GAE [46]
- 3: Jointly optimize the velocity net θ and noise net θ' by taking gradient step on the clipped surrogate loss:

$$\nabla_{\bar{\theta}} \frac{1}{B} \sum_{i=1}^B \left[-\min \left(\frac{\pi_{\bar{\theta}}(\mathbf{a}_i|o_i)}{\pi_{\bar{\theta}_{\text{old}}}(\mathbf{a}_i|o_i)} \hat{A}_i, \text{clip} \left(\frac{\pi_{\bar{\theta}}(\mathbf{a}_i|o_i)}{\pi_{\bar{\theta}_{\text{old}}}(\mathbf{a}_i|o_i)}, 1 - \epsilon, 1 + \epsilon \right) \hat{A}_i \right) + \alpha \cdot \mathcal{R}(\mathbf{a}_i, o_i; \bar{\theta}, \bar{\theta}_{\text{old}}) \right]$$

- 4: **Return** updated parameters θ, θ'
-

4.1 Likelihood Computation over a Short Denoising Trajectory

The log probability of a policy, which quantifies action stochasticity, is essential for policy gradient methods in continuous control [22, 47]. However, computing the log probability for flow-matching policies with minimal denoising steps is challenging.

Although an exact log probability expression exists [11] for continuous-time flow models,

$$\ln p_1(\psi_1(x)) = \ln p_0(\psi_0(x)) - \int_0^1 \nabla \cdot v(t, \psi_t(x)) dt, \quad x \sim p_0(\cdot) \quad (4)$$

in practice, we need to simulate this integral with numerical solvers and estimate the divergence [24]:

$$\widehat{\ln p_1(x_1)} = \ln p_0(x_0) - \sum_{k=0}^{K-1} \text{tr} [Z^\top \partial_X v_\theta(t_i, X_{t_i}) Z] \Delta t_i, \quad (5)$$

where Z is a zero-mean random vector with an identity covariance matrix. However, the trace estimator involves Monte-Carlo error; Simulating the integral introduces discretization error, which becomes more pronounced with larger step sizes (fewer denoising steps) [45]—a critical limitation for fast inference in robotic action generation. Treating the flow process at inference as a discrete-time Markov process can mitigate this issue. However, the intermediate variables follow a deterministic transition $p(X_{t+\Delta t} = x | X_t) = \delta(x - X_t - v_\theta(t, X_t)\Delta t)$, which renders the computation of the probability impossible.

Our approach differs from previous methods by injecting learnable noise directly into the flow model’s trajectory, thereby transforming the flow into a discrete-time Markov process with closed-form transitions. During generation, actions are sampled from a normal distribution whose mean is given by the velocity field and whose standard deviation is parameterized by a noise injection network θ' . For robotic policies, this yields:

$$a^0 \sim \mathcal{N}(0, \mathbb{I}_{d_A}), \quad a^{k+1} \sim \mathcal{N}(\cdot | a^k + v_\theta(t_i, a^k, o)\Delta t_i, \sigma_{\theta'}^2(t_i, a^k, o)) \quad (6)$$

We condition the noise on the current denoised action and time to preserve the Markov property of the flow process. Consequently, the joint log probability of the denoising process admits the following expansion:

$$\ln \pi(a^0, \dots, a^K | o; \theta, \theta') = \ln \mathcal{N}(0, \mathbb{I}_{d_A}) + \sum_{k=0}^{K-1} \ln \mathcal{N}(a^{k+1} | a^k + v_\theta(t_k, a^k, o)\Delta t_k, \sigma_{\theta'}^2(t_k, a^k, o)) \quad (7)$$

where $t_k = \frac{k}{K}$ and $\Delta t_k = \frac{1}{K}$ under uniform discretization.

We treat the flow model at inference as a discrete-time process, and we have complete knowledge of the noise statistics. Unlike the empirical estimate in Eq. (5), the joint probability expression in Eq. (7) is exact, even for arbitrarily large step sizes (or equivalently, minimal denoising steps). This precision guarantees stable fine-tuning of policies, particularly for very few or even one-step inference. By avoiding trace estimation, our method eliminates errors and computational overhead associated with Monte-Carlo estimation.

4.2 Policy Gradient of a Discrete-time Markov Process

Although Eq. (7) provides the joint probability for the discrete-time Markov process that generates the action through denoising, it does not directly describe the marginal probability of the final action that the robot ultimately executes in the environment. Fortunately, we can establish a policy gradient theorem for policies parameterized by a discrete-time Markov process. This enables us to leverage Eq. (7) effectively to optimize the noise-injected flows.

Theorem 4.1 (Policy Gradient Theorem for Markov Process Policy). *For a POMDP with a reactive policy π^θ described by a discrete-time Markov Process $o_h \rightarrow a_h^0 \rightarrow a_h^1 \rightarrow \dots \rightarrow a_h^K = a_h$, the policy gradient is*

$$\nabla_\theta J(\pi^\theta) = \mathbb{E}^{\pi^\theta} \left[\sum_{h=0}^{+\infty} \gamma^h A_h^{\pi^\theta}(o_h, a_h) \nabla_\theta \ln \pi^\theta(a_h^0, a_h^1, \dots, a_h^K | o_h) \right] \quad (8)$$

Further assuming that the policy and POMDP are stationary, the policy gradient takes the form of

$$\nabla_\theta J(\pi^\theta) = \frac{1}{1-\gamma} \mathbb{E}_{o \sim d_\rho^{\pi^\theta}(\cdot)} \mathbb{E}_{a^0, a^1, \dots, a^K \sim \pi^\theta(\cdot | o)} \left[Q^{\pi^\theta}(o, a) \nabla_\theta \sum_{k=0}^{K-1} \ln \pi^\theta(a^{k+1} | a^k, o) \right] \quad (9a)$$

$$= \frac{1}{1-\gamma} \mathbb{E}_{o \sim d_\rho^{\pi^\theta}(\cdot)} \mathbb{E}_{a^0, a^1, \dots, a^K \sim \pi^\theta(\cdot | o)} \left[A^{\pi^\theta}(o, a) \nabla_\theta \sum_{k=0}^{K-1} \ln \pi^\theta(a^{k+1} | a^k, o) \right] \quad (9b)$$

where d_ρ^π is the discounted observation visitation frequency, defined as

$$d_\rho^\pi(o) := (1-\gamma) \mathbb{E}_{s_1 \sim \rho(\cdot)} \left[\sum_{h=0}^{+\infty} \gamma^h p(o_h = o | s_1; \pi) \right] \quad (10)$$

Theorem 4.1 builds on Theorem B.1 in [40] and established results in policy gradient theory [2]. We provide the proofs in Appendix A.

Using Eq. (7), we enable the application of various modern deep policy gradient algorithms to optimize a policy parameterized by a discrete-time Markov process, including the noise-injected flows introduced in Section 4.1, which are of particular interest. Specifically, we can optimize the policy using either Eq. (9a) or Eq. (9b). In this work, we implement Eq. (9b) with the clipped surrogate loss [47] due to its stability.

By combining Eq. (7) with Eq. (9), we derive our algorithm, ‘‘ReinFlow’’, outlined in Alg. 1. We also present one possible policy optimization subroutine in Alg. 2. In Alg. 1, we denote the denoised action sequence a^0, \dots, a^K as a boldfaced \mathbf{a} and represent the combined parameters of the velocity and noise networks as $\bar{\theta} = [\theta, \theta']$.

We also note that, beyond the implementations in Alg. 1 and Alg. 2, we can optimize Eq. (9b) by replacing Eq. (3) with:

$$\theta, \theta' = \underset{\bar{\theta}}{\operatorname{argmin}} \frac{1}{B} \sum_{i=1}^B \left[-Q^{\bar{\theta}_{\text{old}}}(o_i, a_i) \sum_{k=0}^{K-1} \ln \pi^{\bar{\theta}}(a_i^{k+1} | a_i^k, o_i) + \alpha \cdot \mathcal{R}(\mathbf{a}_i, o_i; \bar{\theta}) \right], \text{ where } \bar{\theta} := [\theta, \theta'] \quad (11)$$

and employ off-policy methods, such as SAC [22], to update the policy.

In practice, we adopt ‘‘action chunking’’ during policy execution [29], in which the policy outputs multiple actions in a batch given an observation. We explain how action chunking affects likelihood computation in Appendix A.2.

4.3 Noise Injection Network

The noise has the same shape of the joint torques and is applied to the whole denoising process of action generation. With the noise, we characterize the policy’s probability in closed form. The price we take is a slight increase in noise net parameters, which is only a fraction of the pre-trained policy, as indicated by Table 2.

During fine-tuning, the noise injection network θ' is trained with the velocity network θ to add diversity to the sample path for better exploration. The loss function for θ' is the loss of the policy gradient (Eq. (9)), the same as for the net velocity. After fine-tuning, we discard the noise net θ' and recover the flow matching policy, which is still made up of deterministic maps. By optimizing the noise net, the agent automatically adjusts her exploration level over the course of training.

The noise network could condition on o , (o, t) , or even output fixed constants. We provide a comparative study in Section 6 to analyze how the noise conditions affect ReinFlow’s performance. When the noise injection network is learnable, it uses features from the pre-trained flow policy to save parameters and ensure consistency.

We determine the noise limit using a set of key hyperparameters that vary according to the mechanical structural constraints of each joint. We study the effect of the noise bounds in Section 5. Empirically, we find that when the success rate converges to 100%, the noise level naturally decays. We can also manually control the noise level by adjusting the limits, or even increase the standard deviation of the noise with regularization of the entropy to promote exploration (see Section 4.4).

4.4 Regularization

ReinFlow also supports various ways to regularize the fine-tuned policy.

Wasserstein-2 (W_2) Regularization. One approach is to adopt Wasserstein regularization [28, 38], which constrains the Wasserstein-2 distance from the fine-tuned policy to the pre-trained policy. Studies show that W_2 regularization could improve training stability for generative models [4, 28]. In practice, we minimize a tractable upper bound on this distance to enforce such constraint:

$$\begin{aligned}\mathcal{R}_{W_2}(\theta, \theta_{\text{old}}) &= \mathbb{E}_o \mathbb{E}_{a \sim \pi_\theta(\cdot|o), a_{\text{old}} \sim \pi_{\theta_{\text{old}}}(\cdot|o)} \left[\frac{1}{2} \|a - a_{\text{old}}\|_2^2 \right] \\ &\geq \mathbb{E}_o \left[\inf_{\lambda \in \Lambda} \mathbb{E}_{x, y \sim \lambda_o} \left[\frac{1}{2} \|x - y\|_2^2 \right] \right] := \mathbb{E}_o [W_2^2(\pi_{\theta_{\text{old}}}(\cdot|o), \pi_\theta(\cdot|o))] \end{aligned} \quad (12)$$

In Eq. (12), Λ_o indicates the set of distributions over \mathcal{A}^2 whose marginals are $\pi_{\theta_{\text{old}}}(\cdot|o)$ and $\pi_\theta(\cdot|o)$. To implement Eq. (12), we replace the expectations with the sample mean over a batch of data. Inspired by [38], we integrate a and a_{old} from the same starting noise $a_0 \sim \mathcal{N}(0, \mathbb{I}_{d_A})$, to control the stochasticity of the initial denoise action. We also note that when computing \mathcal{R}_{W_2} , we do not inject noise when sampling a from π_θ .

Entropy Regularization. Another technique is entropy regularization, which theory has shown accelerates convergence [1, 10] and encourages exploration [22] for simple policy classes. For a flow matching policy parameterized with a discrete-time Markov process, we adopt the negative per-symbol entropy rate (or block entropy) [48] as the entropy regularizer. For a stationary POMDP and policy, we define the regularizer as

$$\begin{aligned}\mathcal{R}_h(\bar{\theta}) &:= -\frac{1}{K+1} \mathbb{E} [\mathbf{h}(a^0, a^1, \dots, a^K | o, \bar{\theta})] \\ &= -\frac{1}{K+1} \mathbb{E} \left[\mathbf{h}(\mathcal{N}(0, \mathbb{I}_{d_A})) + \sum_{k=0}^{K-1} \mathbf{h}(\mathcal{N}(a^k + v_\theta(t_k, a^k, o) \Delta t_k, \sigma_{\theta'}^2(t_k, a^k, o))) \right] \end{aligned}$$

Here, the last step is due to the definition of the noise-injected flow process in Eq. (6). \mathbf{h} is the differential entropy operator [14], of which normal distributions possess a simple closed-form expression specified in Section 3. According to [48], the per-symbol entropy measures the Shannon entropy of a finite symbol sequence with long-range correlations. By minimizing \mathcal{R}_h , we promote the agent to seek more diverse actions, enhancing exploration.

We carry out experiments in Section 5 to compare the effects of different regularizations on the performance of ReinFlow. By default, we adopt entropy regularization in Algorithm 1 for state-input tasks and do not adopt regularization for visual manipulation tasks.

5 Experiments

We run simulated robot learning experiments to test the effectiveness and flexibility of our method, ReinFlow. We aim to adopt ReinFlow to significantly enhance the success rate of pre-trained flow

matching policies trained on mediocre expert data. We also managed to fine-tune at very few or even one denoising step for Rectified Flow (indicated by “ReinFlow-R”) and Shortcut Models (indicated by “ReinFlow-S”), where fine-tuning the two types of pre-trained models shares the same training hyperparameters.

We adopt a PPO-based implementation of our algorithm due to its stability. Although alternative implementations may offer higher sample efficiency, we prioritize wall-time efficiency in simulated environments over sample cost. Exploring more sample-efficient RL algorithms for ReinFlow, especially in real-world scenarios where data collection is expensive, is an interesting direction for future work.

We compare ReinFlow against various RL methods for fine-tuning diffusion and flow-based policies, particularly DPPO and FQL. DPPO is a strong online RL algorithm for diffusion policies, developed under a bilevel MDP formulation [42]. FQL represents state-of-the-art offline RL for flow-matching policies and applies to offline-to-online fine-tuning. Comparisons with other baselines are provided in the Appendix E.

5.1 Environment Setup and Data Curation

We compare the algorithms in locomotion and manipulation tasks. In locomotion, the agent receives state input and a dense reward, similar to sim2real RL for legged robots [44]. We also consider manipulation tasks, where agents receive pixel and/or state inputs with sparse rewards.

OpenAI Gym [9]. We fine-tuned flow matching policies with ReinFlow in “Hopper”, “Walker2d”, “Ant” and “Humanoid” where these tasks are listed in ascending difficulty, and the last two involve high-dimensional state inputs and are considered very challenging continuous control problems. Expert data are medium- or medium-expert-level demonstrations collected from the D4RL dataset [19].³

Franka Kitchen [21]. In Franka Kitchen, a Franka robot learns long-horizon multitask planning by completing four state-based manipulation tasks sequentially. We pre-train the models with human teleoperated data with complete, mixed, or partial demonstrations of the four tasks.

Robomimic [36]. We adopt Robomimic visual manipulation tasks: PickPlaceCan (Can), NutAssemblySquare (Square), and TwoArmTransport (Transport). Data are collected via human teleportation and processed following DPPO [42], containing fewer and lower-quality data than proficient human.

5.2 Experiments

ReinFlow demonstrates strong training stability with a significant increase in the success rate or success rate in all tasks. In Gym and Franka Kitchen benchmarks, it achieves the best overall efficiency and performance improvement.

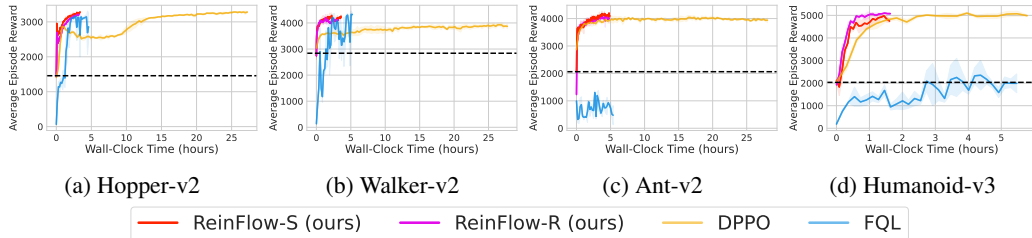


Figure 1: Wall time efficiency in OpenAI Gym. Dashed lines indicate the behavior cloning level.

Across three Robomimic visual manipulation tasks, ReinFlow-S and ReinFlow-R improve the success rate of the pre-trained policy by an average of 45.77%. ReinFlow achieves success rates comparable to DPPO, requiring significantly fewer fine-tuning steps and less wall-clock time. Notably, it uses fewer denoising steps: just *one* in can and square, and a four-step flow in transport, compared to the five-step DDIM used by DPPO.

³Except for "Humanoid" task, where the data is sampled from our own pre-trained SAC agent.

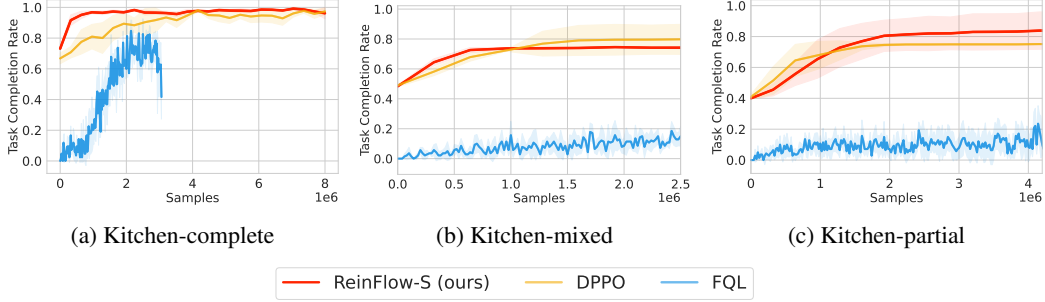


Figure 2: Task completion rates of state-input manipulation tasks in Franka Kitchen

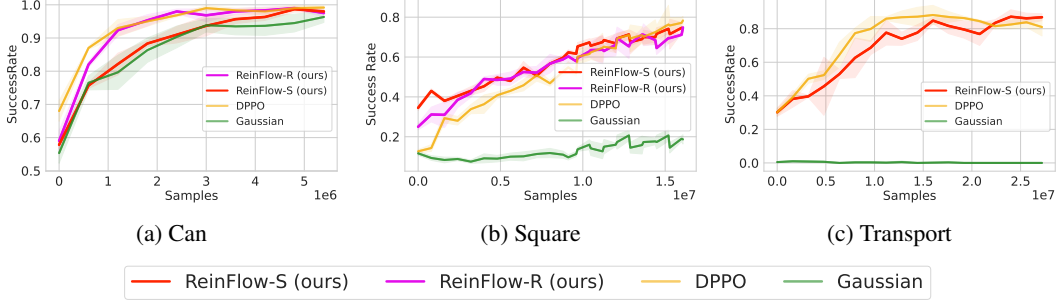


Figure 3: Success rates in visual manipulation tasks in Robomimic.

6 The Design Choice and Key Factors Affecting ReinFlow

This section analyzes how the pre-trained model and denoising steps affect our algorithm. We also study the effects of the noise level, the type, and the intensity of regularization.

Scaling. We fine-tune flow matching policies trained on datasets with different numbers of episodes and test the performance of pre-trained and fine-tuned models at different denoising steps. Fig 4a reveals that scaling inference steps and/or pre-training data quantity does not consistently improve the reward, which is consistent with the findings in [31]. However, ReinFlow consistently improves the success rate or reward over the pre-trained policies regardless of the pre-training scale.

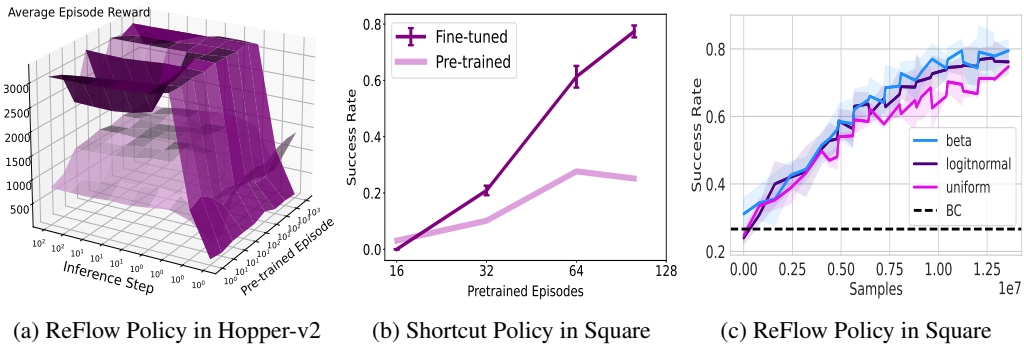
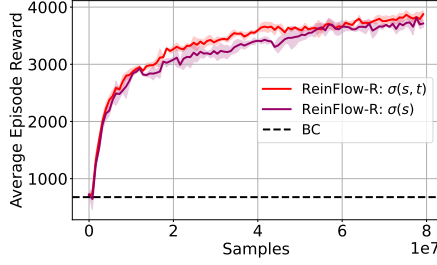


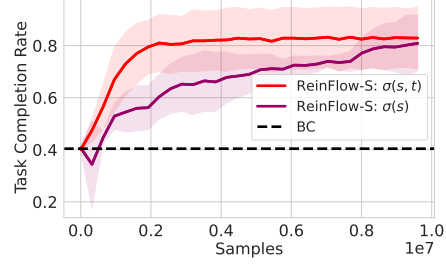
Figure 4: RL offers an orthogonal scaling path beyond data or inference. The gain is invariant to denoising steps—at 4 steps in Hopper and 1 in Square.

Flow Matching’s Time Distribution. The effectiveness of ReinFlow is not affected by altering the time sampling distribution of the pre-trained flow matching policy. However, the beta distribution is slightly stronger when fine-tuning in one denoising step, as in the case in Fig. 4c.

Noise Network Inputs. The inputs of the noise injection network affect the performance of fine-tuned flow policies. As shown in Fig. 5, conditioning both on observations and time often yields a higher success rate, as this approach allows the noise network to learn how to create more diverse actions by altering the noise intensity at different denoising steps.



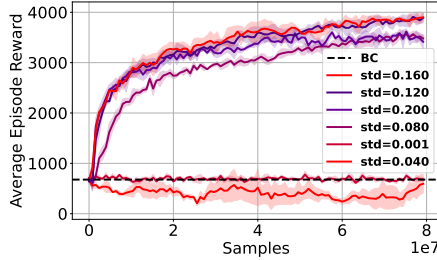
(a) Noise Input's Effect in Ant



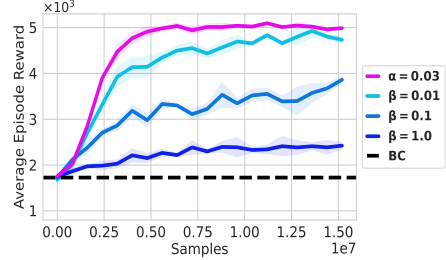
(b) Noise Condition's Effect in Kitchen-partial

Figure 5: Conditioning on state and time yields a higher success rate than only conditioning on states.

Noise Level and Exploration. The noise magnitude is the key factor that influences the performance of ReinFlow. Fig. 6a shows small noise leads to limited exploration, while moderate noise enables rapid improvement, up to three times higher rewards. Beyond this threshold, performance becomes less sensitive to noise. Reducing noise proves beneficial for visuomotor policies, precision-critical tasks, longer denoising chains, and weakly pre-trained models.



(a) Noise Affects Exploration



(b) W_2 (blue) and Entropy (red) Regularization

Figure 6: Effect of noise and regularization in Ant-v0 (left) and Humanoid-v3 (right)

Regularization and Exploration. ReinFlow supports various regularizations. Adding entropy regularization, especially in locomotion tasks, is generally more effective than constraining the policy with a W_2 regularizer. As shown in Fig. 6b, reducing the W_2 coefficient β allows the policy to surpass the behavior cloning baseline and learn more robust actions, approaching the performance achieved with entropy regularization ($\alpha = 0.03$). This also helps explain why the offline RL method FQL, which enforces W_2 constraints during training, underperforms compared to our online approach.

7 Conclusion, Limitations, and Future Work

This work introduces ReinFlow, the first online reinforcement learning (RL) framework that stably fine-tunes a family of flow matching policies for continuous robotic control. In state-input locomotion and visual manipulation tasks, ReinFlow surpasses existing methods that fine-tune diffusion or flow models using RL, while reducing wall-clock time by over 50% compared to the state-of-the-art diffusion RL algorithm. We conducted a sensitivity analysis to identify the key factors affecting ReinFlow's performance.

ReinFlow's current implementation has several limitations. Although the on-policy design saves wall-time with parallelism, future work should explore a sample-efficient implementation and adapting ReinFlow to real-world RL. Another open direction is to reduce its sensitivity to noise magnitude, auto-tune or remove these hyperparameters. Lastly, our current experiments use relatively small networks, and scaling ReinFlow to large flow-based vision-language-action (VLA) models remains an exciting challenge. We leave these to future work.

Acknowledgements This work was supported by National Natural Science Foundation of China (No.62406159, 62325405), Postdoctoral Fellowship Program of CPSF under Grant Number (GZC20240830, 2024M761676), China Postdoctoral Science Special Foundation 2024T170496. The authors are grateful to Shu’ang Yu for reviewing the earlier versions of the paper. We also thank Feng Gao, Cheng Yin, and Ningyuan Yang for many fruitful discussions and comments.

References

- [1] A. Agarwal, N. Jiang, S. M. Kakade, and W. Sun. Reinforcement learning: Theory and algorithms. *CS Dept., UW Seattle, Seattle, WA, USA, Tech. Rep*, 32, 2019.
- [2] A. Agarwal, S. M. Kakade, J. D. Lee, and G. Mahajan. On the theory of policy gradient methods: Optimality, approximation, and distribution shift. *Journal of Machine Learning Research*, 22(98):1–76, 2021.
- [3] L. Ankile, A. Simeonov, I. Shenfeld, and P. Agrawal. Juicer: Data-efficient imitation learning for robotic assembly, 2024.
- [4] M. Arjovsky, S. Chintala, and L. Bottou. Wasserstein generative adversarial networks. In D. Precup and Y. W. Teh, editors, *Proceedings of the 34th International Conference on Machine Learning*, volume 70 of *Proceedings of Machine Learning Research*, pages 214–223. PMLR, 06–11 Aug 2017.
- [5] S. Belkhale, Y. Cui, and D. Sadigh. Data quality in imitation learning. In A. Oh, T. Naumann, A. Globerson, K. Saenko, M. Hardt, and S. Levine, editors, *Advances in Neural Information Processing Systems*, volume 36, pages 80375–80395. Curran Associates, Inc., 2023.
- [6] K. Black, N. Brown, D. Driess, A. Esmail, M. Equi, C. Finn, N. Fusai, L. Groom, K. Hausman, B. Ichter, S. Jakubczak, T. Jones, L. Ke, S. Levine, A. Li-Bell, M. Mothukuri, S. Nair, K. Pertsch, L. X. Shi, J. Tanner, Q. Vuong, A. Walling, H. Wang, and U. Zhilinsky. π_0 : A vision-language-action flow model for general robot control, 2024.
- [7] K. Black, N. Brown, D. Driess, A. Esmail, M. Equi, C. Finn, N. Fusai, L. Groom, K. Hausman, B. Ichter, S. Jakubczak, T. Jones, L. Ke, S. Levine, A. Li-Bell, M. Mothukuri, S. Nair, K. Pertsch, L. X. Shi, J. Tanner, Q. Vuong, A. Walling, H. Wang, and U. Zhilinsky. π_0 : A vision-language-action flow model for general robot control, 2024.
- [8] M. Braun, N. Jaquier, L. Rozo, and T. Asfour. Riemannian flow matching policy for robot motion learning. In *2024 IEEE/RSJ International Conference on Intelligent Robots and Systems (IROS)*, pages 5144–5151, 2024.
- [9] G. Brockman, V. Cheung, L. Pettersson, J. Schneider, J. Schulman, J. Tang, and W. Zaremba. Openai gym, 2016.
- [10] S. Cen, C. Cheng, Y. Chen, Y. Wei, and Y. Chi. Fast global convergence of natural policy gradient methods with entropy regularization. *Oper. Res.*, 70(4):2563–2578, July 2022.
- [11] R. T. Q. Chen, Y. Rubanova, J. Bettencourt, and D. K. Duvenaud. Neural ordinary differential equations. In S. Bengio, H. Wallach, H. Larochelle, K. Grauman, N. Cesa-Bianchi, and R. Garnett, editors, *Advances in Neural Information Processing Systems*, volume 31. Curran Associates, Inc., 2018.
- [12] C. Chi, Z. Xu, S. Feng, E. Cousineau, Y. Du, B. Burchfiel, R. Tedrake, and S. Song. Diffusion policy: Visuomotor policy learning via action diffusion, 2024.
- [13] O. X.-E. Collaboration, A. O’Neill, A. Rehman, A. Gupta, A. Maddukuri, A. Gupta, A. Padalkar, A. Lee, A. Pooley, A. Gupta, A. Mandlekar, A. Jain, A. Tung, A. Bewley, A. Herzog, A. Irpan, A. Khazatsky, A. Rai, A. Gupta, A. Wang, A. Kolobov, A. Singh, A. Garg, A. Kembhavi, A. Xie, A. Brohan, A. Raffin, A. Sharma, A. Yavary, A. Jain, A. Balakrishna, A. Wahid, B. Burgess-Limerick, B. Kim, B. Schölkopf, B. Wulfe, B. Ichter, C. Lu, C. Xu, C. Le, C. Finn, C. Wang, C. Xu, C. Chi, C. Huang, C. Chan, C. Agia, C. Pan, C. Fu, C. Devin, D. Xu, D. Morton, D. Driess, D. Chen, D. Pathak, D. Shah, D. Büchler, D. Jayaraman, D. Kalashnikov, D. Sadigh,

- E. Johns, E. Foster, F. Liu, F. Ceola, F. Xia, F. Zhao, F. V. Frujeri, F. Stulp, G. Zhou, G. S. Sukhatme, G. Salhotra, G. Yan, G. Feng, G. Schiavi, G. Berseth, G. Kahn, G. Yang, G. Wang, H. Su, H.-S. Fang, H. Shi, H. Bao, H. B. Amor, H. I. Christensen, H. Furuta, H. Bharadhwaj, H. Walke, H. Fang, H. Ha, I. Mordatch, I. Radosavovic, I. Leal, J. Liang, J. Abou-Chakra, J. Kim, J. Drake, J. Peters, J. Schneider, J. Hsu, J. Vakil, J. Bohg, J. Bingham, J. Wu, J. Gao, J. Hu, J. Wu, J. Wu, J. Sun, J. Luo, J. Gu, J. Tan, J. Oh, J. Wu, J. Lu, J. Yang, J. Malik, J. Silvério, J. Hejna, J. Booher, J. Tompson, J. Yang, J. Salvador, J. J. Lim, J. Han, K. Wang, K. Rao, K. Pertsch, K. Hausman, K. Go, K. Gopalakrishnan, K. Goldberg, K. Byrne, K. Oslund, K. Kawaharazuka, K. Black, K. Lin, K. Zhang, K. Ehsani, K. Lekkala, K. Ellis, K. Rana, K. Srinivasan, K. Fang, K. P. Singh, K.-H. Zeng, K. Hatch, K. Hsu, L. Itti, L. Y. Chen, L. Pinto, L. Fei-Fei, L. Tan, L. J. Fan, L. Ott, L. Lee, L. Weihs, M. Chen, M. Lepert, M. Memmel, M. Tomizuka, M. Itkina, M. G. Castro, M. Spero, M. Du, M. Ahn, M. C. Yip, M. Zhang, M. Ding, M. Heo, M. K. Srirama, M. Sharma, M. J. Kim, N. Kanazawa, N. Hansen, N. Heess, N. J. Joshi, N. Suenderhauf, N. Liu, N. D. Palo, N. M. M. Shafiullah, O. Mees, O. Kroemer, O. Bastani, P. R. Sanketi, P. T. Miller, P. Yin, P. Wohlhart, P. Xu, P. D. Fagan, P. Mitrano, P. Sermanet, P. Abbeel, P. Sundaresan, Q. Chen, Q. Vuong, R. Rafailov, R. Tian, R. Doshi, R. Mart'in-Mart'in, R. Bajjal, R. Scalise, R. Hendrix, R. Lin, R. Qian, R. Zhang, R. Mendonca, R. Shah, R. Hoque, R. Julian, S. Bustamante, S. Kirmani, S. Levine, S. Lin, S. Moore, S. Bahl, S. Dass, S. Sonawani, S. Tulsiani, S. Song, S. Xu, S. Haldar, S. Karamcheti, S. Adebola, S. Guist, S. Nasiriany, S. Schaal, S. Welker, S. Tian, S. Ramamoorthy, S. Dasari, S. Belkhale, S. Park, S. Nair, S. Mirchandani, T. Osa, T. Gupta, T. Harada, T. Matsushima, T. Xiao, T. Kollar, T. Yu, T. Ding, T. Davchev, T. Z. Zhao, T. Armstrong, T. Darrell, T. Chung, V. Jain, V. Kumar, V. Vanhoucke, W. Zhan, W. Zhou, W. Burgard, X. Chen, X. Chen, X. Wang, X. Zhu, X. Geng, X. Liu, X. Liangwei, X. Li, Y. Pang, Y. Lu, Y. J. Ma, Y. Kim, Y. Chebotar, Y. Zhou, Y. Zhu, Y. Wu, Y. Xu, Y. Wang, Y. Bisk, Y. Dou, Y. Cho, Y. Lee, Y. Cui, Y. Cao, Y.-H. Wu, Y. Tang, Y. Zhu, Y. Zhang, Y. Jiang, Y. Li, Y. Li, Y. Iwasawa, Y. Matsuo, Z. Ma, Z. Xu, Z. J. Cui, Z. Zhang, Z. Fu, and Z. Lin. Open X-Embodiment: Robotic learning datasets and RT-X models. <https://arxiv.org/abs/2310.08864>, 2023.
- [14] T. M. Cover. *Elements of information theory*. John Wiley & Sons, 1999.
- [15] A. Dosovitskiy, L. Beyer, A. Kolesnikov, D. Weissenborn, X. Zhai, T. Unterthiner, M. Dehghani, M. Minderer, G. Heigold, S. Gelly, J. Uszkoreit, and N. Houlsby. An image is worth 16x16 words: Transformers for image recognition at scale. In *International Conference on Learning Representations*, 2021.
- [16] P. Esser, S. Kulal, A. Blattmann, R. Entezari, J. Müller, H. Saini, Y. Levi, D. Lorenz, A. Sauer, F. Boesel, et al. Scaling rectified flow transformers for high-resolution image synthesis. In *Forty-first international conference on machine learning*, 2024.
- [17] J. Fan, S. Shen, C. Cheng, Y. Chen, C. Liang, and G. Liu. Online reward-weighted fine-tuning of flow matching with wasserstein regularization, 2025.
- [18] K. Frans, D. Hafner, S. Levine, and P. Abbeel. One step diffusion via shortcut models. *arXiv preprint arXiv:2410.12557*, 2024.
- [19] J. Fu, A. Kumar, O. Nachum, G. Tucker, and S. Levine. D4{rl}: Datasets for deep data-driven reinforcement learning, 2021.
- [20] Y. Guo, J. Gao, Z. Wu, C. Shi, and J. Chen. Reinforcement learning with demonstrations from mismatched task under sparse reward. In K. Liu, D. Kulic, and J. Ichnowski, editors, *Proceedings of The 6th Conference on Robot Learning*, volume 205 of *Proceedings of Machine Learning Research*, pages 1146–1156. PMLR, 14–18 Dec 2023.
- [21] A. Gupta, V. Kumar, C. Lynch, S. Levine, and K. Hausman. Relay policy learning: Solving long-horizon tasks via imitation and reinforcement learning. In L. P. Kaelbling, D. Kragic, and K. Sugiura, editors, *Proceedings of the Conference on Robot Learning*, volume 100 of *Proceedings of Machine Learning Research*, pages 1025–1037. PMLR, 30 Oct–01 Nov 2020.
- [22] T. Haarnoja, A. Zhou, P. Abbeel, and S. Levine. Soft actor-critic: Off-policy maximum entropy deep reinforcement learning with a stochastic actor. In J. Dy and A. Krause, editors, *Proceedings of the 35th International Conference on Machine Learning*, volume 80 of *Proceedings of Machine Learning Research*, pages 1861–1870. PMLR, 10–15 Jul 2018.

- [23] P. Hansen-Estruch, I. Kostrikov, M. Janner, J. G. Kuba, and S. Levine. Idql: Implicit q-learning as an actor-critic method with diffusion policies, 2023.
- [24] M. F. Hutchinson. A stochastic estimator of the trace of the influence matrix for laplacian smoothing splines. *Communications in Statistics-Simulation and Computation*, 18(3):1059–1076, 1989.
- [25] M. Janner, Y. Du, J. B. Tenenbaum, and S. Levine. Planning with diffusion for flexible behavior synthesis. In *International Conference on Machine Learning*, 2022.
- [26] D. P. Kingma and J. Ba. Adam: A method for stochastic optimization, 2017.
- [27] W. Kong, Q. Tian, Z. Zhang, R. Min, Z. Dai, J. Zhou, J. Xiong, X. Li, B. Wu, J. Zhang, K. Wu, Q. Lin, J. Yuan, Y. Long, A. Wang, A. Wang, C. Li, D. Huang, F. Yang, H. Tan, H. Wang, J. Song, J. Bai, J. Wu, J. Xue, J. Wang, K. Wang, M. Liu, P. Li, S. Li, W. Wang, W. Yu, X. Deng, Y. Li, Y. Chen, Y. Cui, Y. Peng, Z. Yu, Z. He, Z. Xu, Z. Zhou, Z. Xu, Y. Tao, Q. Lu, S. Liu, D. Zhou, H. Wang, Y. Yang, D. Wang, Y. Liu, J. Jiang, and C. Zhong. Hunyuanvideo: A systematic framework for large video generative models, 2025.
- [28] A. Korotin, V. Egiazarian, A. Asadulaev, A. Safin, and E. Burnaev. Wasserstein-2 generative networks. In *International Conference on Learning Representations*, 2021.
- [29] L. Lai, A. Z. Huang, and S. J. Gershman. Action chunking as conditional policy compression, Sep 2022.
- [30] S. Li, R. Krohn, T. Chen, A. Ajay, P. Agrawal, and G. Chalvatzaki. Learning multimodal behaviors from scratch with diffusion policy gradient. *Advances in Neural Information Processing Systems*, 37:38456–38479, 2024.
- [31] F. Lin, Y. Hu, P. Sheng, C. Wen, J. You, and Y. Gao. Data scaling laws in imitation learning for robotic manipulation. In *The Thirteenth International Conference on Learning Representations*, 2025.
- [32] Y. Lipman, R. T. Q. Chen, H. Ben-Hamu, M. Nickel, and M. Le. Flow matching for generative modeling. In *The Eleventh International Conference on Learning Representations*, 2023.
- [33] J. Liu, G. Liu, J. Liang, Y. Li, J. Liu, X. Wang, P. Wan, D. Zhang, and W. Ouyang. Flow-grpo: Training flow matching models via online rl, 2025.
- [34] X. Liu, C. Gong, and Q. Liu. Flow straight and fast: Learning to generate and transfer data with rectified flow. *arXiv preprint arXiv:2209.03003*, 2022.
- [35] I. Loshchilov and F. Hutter. Sgdr: Stochastic gradient descent with restarts. *CoRR*, abs/1608.03983, 2016.
- [36] A. Mandlekar, D. Xu, J. Wong, S. Nasiriany, C. Wang, R. Kulkarni, L. Fei-Fei, S. Savarese, Y. Zhu, and R. Martín-Martín. What matters in learning from offline human demonstrations for robot manipulation. In A. Faust, D. Hsu, and G. Neumann, editors, *Proceedings of the 5th Conference on Robot Learning*, volume 164 of *Proceedings of Machine Learning Research*, pages 1678–1690. PMLR, 08–11 Nov 2022.
- [37] D. Misra. Mish: A self regularized non-monotonic activation function, 2020.
- [38] S. Park, Q. Li, and S. Levine. Flow q-learning, 2025.
- [39] T. Pearce, T. Rashid, A. Kanervisto, D. Bignell, M. Sun, R. Georgescu, S. V. Macua, S. Z. Tan, I. Momennejad, K. Hofmann, and S. Devlin. Imitating human behaviour with diffusion models, 2023.
- [40] M. Psenka, A. Escontrela, P. Abbeel, and Y. Ma. Learning a diffusion model policy from rewards via q-score matching, 2024.
- [41] M. Psenka, A. Escontrela, P. Abbeel, and Y. Ma. Learning a diffusion model policy from rewards via q-score matching, 2025.

- [42] A. Z. Ren, J. Lidard, L. L. Ankile, A. Simeonov, P. Agrawal, A. Majumdar, B. Burchfiel, H. Dai, and M. Simchowitz. Diffusion policy optimization, 2024.
- [43] M. Reuss, M. Li, X. Jia, and R. Lioutikov. Goal-conditioned imitation learning using score-based diffusion policies, 2023.
- [44] N. Rudin, D. Hoeller, P. Reist, and M. Hutter. Learning to walk in minutes using massively parallel deep reinforcement learning. In *Conference on Robot Learning*, pages 91–100. PMLR, 2022.
- [45] T. Sauer. *Numerical analysis*. Addison-Wesley Publishing Company, 2011.
- [46] J. Schulman, P. Moritz, S. Levine, M. Jordan, and P. Abbeel. High-dimensional continuous control using generalized advantage estimation, 2018.
- [47] J. Schulman, F. Wolski, P. Dhariwal, A. Radford, and O. Klimov. Proximal policy optimization algorithms, 2017.
- [48] T. Schürmann and P. Grassberger. Entropy estimation of symbol sequences. *Chaos: An Interdisciplinary Journal of Nonlinear Science*, 6(3):414–427, 1996.
- [49] M. Simchowitz, D. Pfrommer, and A. Jadbabaie. The pitfalls of imitation learning when actions are continuous, 2025.
- [50] A. Sridhar, D. Shah, C. Glossop, and S. Levine. Nomad: Goal masked diffusion policies for navigation and exploration, 2023.
- [51] R. S. Sutton and A. G. Barto. *Reinforcement learning: An introduction*. MIT press, 2018.
- [52] T. Wan, A. Wang, B. Ai, B. Wen, C. Mao, C.-W. Xie, D. Chen, F. Yu, H. Zhao, J. Yang, J. Zeng, J. Wang, J. Zhang, J. Zhou, J. Wang, J. Chen, K. Zhu, K. Zhao, K. Yan, L. Huang, M. Feng, N. Zhang, P. Li, P. Wu, R. Chu, R. Feng, S. Zhang, S. Sun, T. Fang, T. Wang, T. Gui, T. Weng, T. Shen, W. Lin, W. Wang, W. Wang, W. Zhou, W. Wang, W. Shen, W. Yu, X. Shi, X. Huang, X. Xu, Y. Kou, Y. Lv, Y. Li, Y. Liu, Y. Wang, Y. Zhang, Y. Huang, Y. Li, Y. Wu, Y. Liu, Y. Pan, Y. Zheng, Y. Hong, Y. Shi, Y. Feng, Z. Jiang, Z. Han, Z.-F. Wu, and Z. Liu. Wan: Open and advanced large-scale video generative models, 2025.
- [53] L. Wang, J. Zhao, Y. Du, E. H. Adelson, and R. Tedrake. Poco: Policy composition from and for heterogeneous robot learning, 2024.
- [54] Z. Wang, J. J. Hunt, and M. Zhou. Diffusion policies as an expressive policy class for offline reinforcement learning, 2023.
- [55] L. Yang, Z. Huang, F. Lei, Y. Zhong, Y. Yang, C. Fang, S. Wen, B. Zhou, and Z. Lin. Policy representation via diffusion probability model for reinforcement learning, 2023.
- [56] Y. Ze, G. Zhang, K. Zhang, C. Hu, M. Wang, and H. Xu. 3d diffusion policy: Generalizable visuomotor policy learning via simple 3d representations, 2024.
- [57] F. Zhang and M. Gienger. Affordance-based robot manipulation with flow matching, 2025.
- [58] Q. Zheng, M. Le, N. Shaul, Y. Lipman, A. Grover, and R. T. Q. Chen. Guided flows for generative modeling and decision making, 2023.

NeurIPS Paper Checklist

The checklist is designed to encourage best practices for responsible machine learning research, addressing issues of reproducibility, transparency, research ethics, and societal impact. Do not remove the checklist: **The papers not including the checklist will be desk rejected.** The checklist should follow the references and follow the (optional) supplemental material. The checklist does NOT count towards the page limit.

Please read the checklist guidelines carefully for information on how to answer these questions. For each question in the checklist:

- You should answer [Yes], [No], or [NA].
- [NA] means either that the question is Not Applicable for that particular paper or the relevant information is Not Available.
- Please provide a short (1–2 sentence) justification right after your answer (even for NA).

The checklist answers are an integral part of your paper submission. They are visible to the reviewers, area chairs, senior area chairs, and ethics reviewers. You will be asked to also include it (after eventual revisions) with the final version of your paper, and its final version will be published with the paper.

The reviewers of your paper will be asked to use the checklist as one of the factors in their evaluation. While "[Yes]" is generally preferable to "[No]", it is perfectly acceptable to answer "[No]" provided a proper justification is given (e.g., "error bars are not reported because it would be too computationally expensive" or "we were unable to find the license for the dataset we used"). In general, answering "[No]" or "[NA]" is not grounds for rejection. While the questions are phrased in a binary way, we acknowledge that the true answer is often more nuanced, so please just use your best judgment and write a justification to elaborate. All supporting evidence can appear either in the main paper or the supplemental material, provided in appendix. If you answer [Yes] to a question, in the justification please point to the section(s) where related material for the question can be found.

IMPORTANT, please:

- **Delete this instruction block, but keep the section heading “NeurIPS Paper Checklist”,**
- **Keep the checklist subsection headings, questions/answers and guidelines below.**
- **Do not modify the questions and only use the provided macros for your answers.**

1. Claims

Question: Do the main claims made in the abstract and introduction accurately reflect the paper’s contributions and scope?

Answer: YES

Justification: The claims are derived from experiments which is reproduceable.

Guidelines:

- The answer NA means that the abstract and introduction do not include the claims made in the paper.
- The abstract and/or introduction should clearly state the claims made, including the contributions made in the paper and important assumptions and limitations. A No or NA answer to this question will not be perceived well by the reviewers.
- The claims made should match theoretical and experimental results, and reflect how much the results can be expected to generalize to other settings.
- It is fine to include aspirational goals as motivation as long as it is clear that these goals are not attained by the paper.

2. Limitations

Question: Does the paper discuss the limitations of the work performed by the authors?

Answer: [Yes]

Justification: See the last section.

Guidelines:

- The answer NA means that the paper has no limitation while the answer No means that the paper has limitations, but those are not discussed in the paper.
- The authors are encouraged to create a separate "Limitations" section in their paper.
- The paper should point out any strong assumptions and how robust the results are to violations of these assumptions (e.g., independence assumptions, noiseless settings, model well-specification, asymptotic approximations only holding locally). The authors should reflect on how these assumptions might be violated in practice and what the implications would be.
- The authors should reflect on the scope of the claims made, e.g., if the approach was only tested on a few datasets or with a few runs. In general, empirical results often depend on implicit assumptions, which should be articulated.
- The authors should reflect on the factors that influence the performance of the approach. For example, a facial recognition algorithm may perform poorly when image resolution is low or images are taken in low lighting. Or a speech-to-text system might not be used reliably to provide closed captions for online lectures because it fails to handle technical jargon.
- The authors should discuss the computational efficiency of the proposed algorithms and how they scale with dataset size.
- If applicable, the authors should discuss possible limitations of their approach to address problems of privacy and fairness.
- While the authors might fear that complete honesty about limitations might be used by reviewers as grounds for rejection, a worse outcome might be that reviewers discover limitations that aren't acknowledged in the paper. The authors should use their best judgment and recognize that individual actions in favor of transparency play an important role in developing norms that preserve the integrity of the community. Reviewers will be specifically instructed to not penalize honesty concerning limitations.

3. Theory assumptions and proofs

Question: For each theoretical result, does the paper provide the full set of assumptions and a complete (and correct) proof?

Answer: [\[Yes\]](#)

Justification: See the proof in appendix.

Guidelines:

- The answer NA means that the paper does not include theoretical results.
- All the theorems, formulas, and proofs in the paper should be numbered and cross-referenced.
- All assumptions should be clearly stated or referenced in the statement of any theorems.
- The proofs can either appear in the main paper or the supplemental material, but if they appear in the supplemental material, the authors are encouraged to provide a short proof sketch to provide intuition.
- Inversely, any informal proof provided in the core of the paper should be complemented by formal proofs provided in appendix or supplemental material.
- Theorems and Lemmas that the proof relies upon should be properly referenced.

4. Experimental result reproducibility

Question: Does the paper fully disclose all the information needed to reproduce the main experimental results of the paper to the extent that it affects the main claims and/or conclusions of the paper (regardless of whether the code and data are provided or not)?

Answer: [\[Yes\]](#) .

Justification: in appendix.

Guidelines:

- The answer NA means that the paper does not include experiments.

- If the paper includes experiments, a No answer to this question will not be perceived well by the reviewers: Making the paper reproducible is important, regardless of whether the code and data are provided or not.
- If the contribution is a dataset and/or model, the authors should describe the steps taken to make their results reproducible or verifiable.
- Depending on the contribution, reproducibility can be accomplished in various ways. For example, if the contribution is a novel architecture, describing the architecture fully might suffice, or if the contribution is a specific model and empirical evaluation, it may be necessary to either make it possible for others to replicate the model with the same dataset, or provide access to the model. In general, releasing code and data is often one good way to accomplish this, but reproducibility can also be provided via detailed instructions for how to replicate the results, access to a hosted model (e.g., in the case of a large language model), releasing of a model checkpoint, or other means that are appropriate to the research performed.
- While NeurIPS does not require releasing code, the conference does require all submissions to provide some reasonable avenue for reproducibility, which may depend on the nature of the contribution. For example
 - (a) If the contribution is primarily a new algorithm, the paper should make it clear how to reproduce that algorithm.
 - (b) If the contribution is primarily a new model architecture, the paper should describe the architecture clearly and fully.
 - (c) If the contribution is a new model (e.g., a large language model), then there should either be a way to access this model for reproducing the results or a way to reproduce the model (e.g., with an open-source dataset or instructions for how to construct the dataset).
 - (d) We recognize that reproducibility may be tricky in some cases, in which case authors are welcome to describe the particular way they provide for reproducibility. In the case of closed-source models, it may be that access to the model is limited in some way (e.g., to registered users), but it should be possible for other researchers to have some path to reproducing or verifying the results.

5. Open access to data and code

Question: Does the paper provide open access to the data and code, with sufficient instructions to faithfully reproduce the main experimental results, as described in supplemental material?

Answer: [\[Yes\]](#) .

Justification: Will be released few weeks later.

Guidelines:

- The answer NA means that paper does not include experiments requiring code.
- Please see the NeurIPS code and data submission guidelines (<https://nips.cc/public/guides/CodeSubmissionPolicy>) for more details.
- While we encourage the release of code and data, we understand that this might not be possible, so “No” is an acceptable answer. Papers cannot be rejected simply for not including code, unless this is central to the contribution (e.g., for a new open-source benchmark).
- The instructions should contain the exact command and environment needed to run to reproduce the results. See the NeurIPS code and data submission guidelines (<https://nips.cc/public/guides/CodeSubmissionPolicy>) for more details.
- The authors should provide instructions on data access and preparation, including how to access the raw data, preprocessed data, intermediate data, and generated data, etc.
- The authors should provide scripts to reproduce all experimental results for the new proposed method and baselines. If only a subset of experiments are reproducible, they should state which ones are omitted from the script and why.
- At submission time, to preserve anonymity, the authors should release anonymized versions (if applicable).

- Providing as much information as possible in supplemental material (appended to the paper) is recommended, but including URLs to data and code is permitted.

6. Experimental setting/details

Question: Does the paper specify all the training and test details (e.g., data splits, hyper-parameters, how they were chosen, type of optimizer, etc.) necessary to understand the results?

Answer: [\[Yes\]](#) .

Justification: In appendix.

Guidelines:

- The answer NA means that the paper does not include experiments.
- The experimental setting should be presented in the core of the paper to a level of detail that is necessary to appreciate the results and make sense of them.
- The full details can be provided either with the code, in appendix, or as supplemental material.

7. Experiment statistical significance

Question: Does the paper report error bars suitably and correctly defined or other appropriate information about the statistical significance of the experiments?

Answer: [\[Yes\]](#) .

Justification: Results all have shadings by default indicate 1-sigma range.

Guidelines:

- The answer NA means that the paper does not include experiments.
- The authors should answer "Yes" if the results are accompanied by error bars, confidence intervals, or statistical significance tests, at least for the experiments that support the main claims of the paper.
- The factors of variability that the error bars are capturing should be clearly stated (for example, train/test split, initialization, random drawing of some parameter, or overall run with given experimental conditions).
- The method for calculating the error bars should be explained (closed form formula, call to a library function, bootstrap, etc.)
- The assumptions made should be given (e.g., Normally distributed errors).
- It should be clear whether the error bar is the standard deviation or the standard error of the mean.
- It is OK to report 1-sigma error bars, but one should state it. The authors should preferably report a 2-sigma error bar than state that they have a 96% CI, if the hypothesis of Normality of errors is not verified.
- For asymmetric distributions, the authors should be careful not to show in tables or figures symmetric error bars that would yield results that are out of range (e.g. negative error rates).
- If error bars are reported in tables or plots, The authors should explain in the text how they were calculated and reference the corresponding figures or tables in the text.

8. Experiments compute resources

Question: For each experiment, does the paper provide sufficient information on the computer resources (type of compute workers, memory, time of execution) needed to reproduce the experiments?

Answer: [\[Yes\]](#) .

Justification: See appendix.

Guidelines:

- The answer NA means that the paper does not include experiments.
- The paper should indicate the type of compute workers CPU or GPU, internal cluster, or cloud provider, including relevant memory and storage.

- The paper should provide the amount of compute required for each of the individual experimental runs as well as estimate the total compute.
- The paper should disclose whether the full research project required more compute than the experiments reported in the paper (e.g., preliminary or failed experiments that didn't make it into the paper).

9. Code of ethics

Question: Does the research conducted in the paper conform, in every respect, with the NeurIPS Code of Ethics <https://neurips.cc/public/EthicsGuidelines?>

Answer: [Yes] ,

Justification: We are doing what NIPS asks us to do.

Guidelines:

- The answer NA means that the authors have not reviewed the NeurIPS Code of Ethics.
- If the authors answer No, they should explain the special circumstances that require a deviation from the Code of Ethics.
- The authors should make sure to preserve anonymity (e.g., if there is a special consideration due to laws or regulations in their jurisdiction).

10. Broader impacts

Question: Does the paper discuss both potential positive societal impacts and negative societal impacts of the work performed?

Answer: [Yes] .

Justification: Provided in appendix.

Guidelines:

- The answer NA means that there is no societal impact of the work performed.
- If the authors answer NA or No, they should explain why their work has no societal impact or why the paper does not address societal impact.
- Examples of negative societal impacts include potential malicious or unintended uses (e.g., disinformation, generating fake profiles, surveillance), fairness considerations (e.g., deployment of technologies that could make decisions that unfairly impact specific groups), privacy considerations, and security considerations.
- The conference expects that many papers will be foundational research and not tied to particular applications, let alone deployments. However, if there is a direct path to any negative applications, the authors should point it out. For example, it is legitimate to point out that an improvement in the quality of generative models could be used to generate deepfakes for disinformation. On the other hand, it is not needed to point out that a generic algorithm for optimizing neural networks could enable people to train models that generate Deepfakes faster.
- The authors should consider possible harms that could arise when the technology is being used as intended and functioning correctly, harms that could arise when the technology is being used as intended but gives incorrect results, and harms following from (intentional or unintentional) misuse of the technology.
- If there are negative societal impacts, the authors could also discuss possible mitigation strategies (e.g., gated release of models, providing defenses in addition to attacks, mechanisms for monitoring misuse, mechanisms to monitor how a system learns from feedback over time, improving the efficiency and accessibility of ML).

11. Safeguards

Question: Does the paper describe safeguards that have been put in place for responsible release of data or models that have a high risk for misuse (e.g., pretrained language models, image generators, or scraped datasets)?

Answer: [No]

Justification: Open source data.

Guidelines:

- The answer NA means that the paper poses no such risks.

- Released models that have a high risk for misuse or dual-use should be released with necessary safeguards to allow for controlled use of the model, for example by requiring that users adhere to usage guidelines or restrictions to access the model or implementing safety filters.
- Datasets that have been scraped from the Internet could pose safety risks. The authors should describe how they avoided releasing unsafe images.
- We recognize that providing effective safeguards is challenging, and many papers do not require this, but we encourage authors to take this into account and make a best faith effort.

12. Licenses for existing assets

Question: Are the creators or original owners of assets (e.g., code, data, models), used in the paper, properly credited and are the license and terms of use explicitly mentioned and properly respected?

Answer: [\[Yes\]](#)

Justification: Will be disclosed in the appendix.

Guidelines:

- The answer NA means that the paper does not use existing assets.
- The authors should cite the original paper that produced the code package or dataset.
- The authors should state which version of the asset is used and, if possible, include a URL.
- The name of the license (e.g., CC-BY 4.0) should be included for each asset.
- For scraped data from a particular source (e.g., website), the copyright and terms of service of that source should be provided.
- If assets are released, the license, copyright information, and terms of use in the package should be provided. For popular datasets, paperswithcode.com/datasets has curated licenses for some datasets. Their licensing guide can help determine the license of a dataset.
- For existing datasets that are re-packaged, both the original license and the license of the derived asset (if it has changed) should be provided.
- If this information is not available online, the authors are encouraged to reach out to the asset's creators.

13. New assets

Question: Are new assets introduced in the paper well documented and is the documentation provided alongside the assets?

Answer: [\[Yes\]](#) .

Justification: In appendix.

Guidelines:

- The answer NA means that the paper does not release new assets.
- Researchers should communicate the details of the dataset/code/model as part of their submissions via structured templates. This includes details about training, license, limitations, etc.
- The paper should discuss whether and how consent was obtained from people whose asset is used.
- At submission time, remember to anonymize your assets (if applicable). You can either create an anonymized URL or include an anonymized zip file.

14. Crowdsourcing and research with human subjects

Question: For crowdsourcing experiments and research with human subjects, does the paper include the full text of instructions given to participants and screenshots, if applicable, as well as details about compensation (if any)?

Answer: [\[No\]](#) .

Justification: No such experiments.

Guidelines:

- The answer NA means that the paper does not involve crowdsourcing nor research with human subjects.
- Including this information in the supplemental material is fine, but if the main contribution of the paper involves human subjects, then as much detail as possible should be included in the main paper.
- According to the NeurIPS Code of Ethics, workers involved in data collection, curation, or other labor should be paid at least the minimum wage in the country of the data collector.

15. Institutional review board (IRB) approvals or equivalent for research with human subjects

Question: Does the paper describe potential risks incurred by study participants, whether such risks were disclosed to the subjects, and whether Institutional Review Board (IRB) approvals (or an equivalent approval/review based on the requirements of your country or institution) were obtained?

Answer: [No] .

Justification: No such risk.

Guidelines:

- The answer NA means that the paper does not involve crowdsourcing nor research with human subjects.
- Depending on the country in which research is conducted, IRB approval (or equivalent) may be required for any human subjects research. If you obtained IRB approval, you should clearly state this in the paper.
- We recognize that the procedures for this may vary significantly between institutions and locations, and we expect authors to adhere to the NeurIPS Code of Ethics and the guidelines for their institution.
- For initial submissions, do not include any information that would break anonymity (if applicable), such as the institution conducting the review.

16. Declaration of LLM usage

Question: Does the paper describe the usage of LLMs if it is an important, original, or non-standard component of the core methods in this research? Note that if the LLM is used only for writing, editing, or formatting purposes and does not impact the core methodology, scientific rigorousness, or originality of the research, declaration is not required.

Answer: [Yes] .

Justification: In OpenReview webpage.

Guidelines:

- The answer NA means that the core method development in this research does not involve LLMs as any important, original, or non-standard components.
- Please refer to our LLM policy (<https://neurips.cc/Conferences/2025/LLM>) for what should or should not be described.

We provide a schematic in Fig 7 to illustrate the procedure of fine-tuning a flow matching policy with ReinFlow.

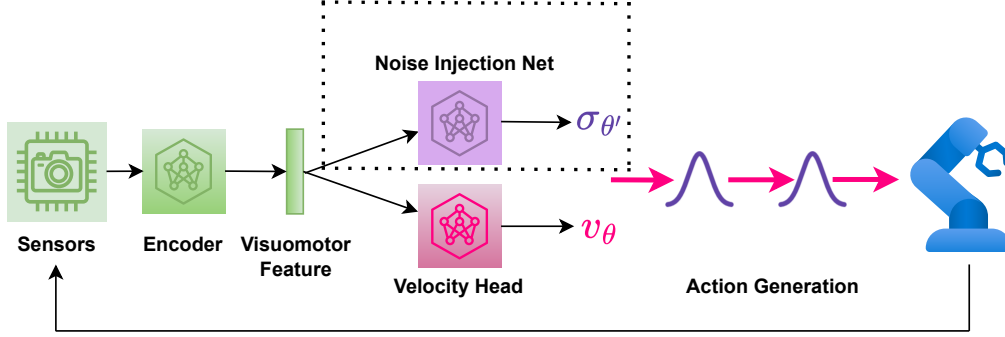


Figure 7: Fine-tuning a flow matching policy with online RL algorithm ReinFlow (Alg. 1).

Through interactions with the environment, the robot collects visual and proprioceptive signals, from which a pre-trained policy extracts features and outputs the velocity field of the following action, v_θ . A noise injection network $\sigma_{\theta'}$ shares the extracted features with v_θ and outputs a Gaussian noise that smoothenes the flow’s deterministic ODE path, converting flows to a discrete-time Markov process with Gaussian transition probabilities. The noise injection yields an exact and straightforward likelihood expression at any denoising steps, which is friendly for policy gradient optimization. The noise injection net $\sigma_{\theta'}$, surrounded by the dot lines, co-trained with v_θ but will be discarded after fine-tuning. The size of $\sigma_{\theta'}$ is only a fraction of the pre-trained flow policy. We outline our findings on a webpage: <https://reinflow.github.io/>. In what follows, we provide the theoretical background of our algorithm, report the findings omitted by the main text, and elaborate on the implementation details required to reproduce our experimental results.

A Theoretical Support

A.1 Proof of Theorem 4.1

In this section, we prove Theorem 4.1, the policy gradient theorem for discrete-time Markov process policies.

For notation simplicity, we only consider an infinite-horizon POMDP with a reactive policy. We obtain the result for the finite-horizon setting by imposing $r_h = 0$ for h larger than the finite horizon H . For the reader’s convenience, we recall several fundamental definitions of RL. The objective function for RL is given by $J(\pi) = \mathbb{E}^\pi \left[\sum_{h=0}^{+\infty} \gamma^h r_h(o_h, a_h) \right]$, The value function, Q function, and the advantage functions are defined as

$$\begin{aligned} V_h^\pi(o_h) &:= \mathbb{E}^\pi \left[\sum_{\tau=h}^{+\infty} \gamma^{\tau-h} r_\tau(a_\tau, o_\tau) \mid o_h \right] \\ Q_h^\pi(o_h, a_h) &:= \mathbb{E}^\pi \left[\sum_{\tau=h}^{+\infty} \gamma^{\tau-h} r_\tau(a_\tau, o_\tau) \mid o_h, a_h \right] \\ A_h^\pi(o_h, a_h) &:= Q_h^\pi(o_h, a_h) - V_h^\pi(o_h) \end{aligned} \quad (13)$$

We first show that we can express the policy gradient for POMDP in terms of the advantage function and the action log probability’s gradient:

$$\nabla_\theta J(\pi^\theta) = \mathbb{E}^{\pi^\theta} \left[\sum_{\tau=0}^{+\infty} \gamma^\tau A_\tau^{\pi^\theta}(o_\tau, a_\tau) \nabla_\theta \ln \pi_\theta(a_\tau | o_\tau) \right] \quad (14)$$

Remark A.1. In Eq. (14), we use θ to indicate general policy parameters. θ should be understood as $\bar{\theta} = [\theta, \theta']$, that is, the combination of the velocity and noise nets when we instantiate the policy as a noise-injected flow matching policy.

Proof.

$$\begin{aligned}
\nabla_\theta J(\pi^\theta) &= \sum_{h=0}^{+\infty} \gamma^h \int_{\mathcal{O} \times \mathcal{A}^h} r_h(o_h, a_h) \cdot \nabla_\theta p(o_{1:h}, a_{1:h} | \pi^\theta) \\
&= \sum_{h=0}^{+\infty} \gamma^h \int_{\mathcal{O} \times \mathcal{A}^h} r_h(o_h, a_h) \cdot \nabla_\theta \exp \ln p(o_{1:h}, a_{1:h} | \pi^\theta) \\
&= \sum_{h=0}^{+\infty} \gamma^h \int_{\mathcal{O} \times \mathcal{A}^h} r_h(o_h, a_h) \cdot p(o_{1:h}, a_{1:h} | \pi^\theta) \nabla_\theta \ln p(o_{1:h}, a_{1:h} | \pi^\theta) \\
&\stackrel{(i)}{=} \sum_{h=0}^{+\infty} \gamma^h \int_{\mathcal{O} \times \mathcal{A}^h} r_h(o_h, a_h) \cdot p(o_{1:h}, a_{1:h} | \pi^\theta) \sum_{\tau=1}^h \nabla_\theta \ln \pi_\theta(a_\tau | o_\tau) \\
&= \mathbb{E}^{\pi^\theta} \left[\sum_{h=0}^{+\infty} \gamma^h r_h(o_h, a_h) \sum_{\tau=1}^h \nabla_\theta \ln \pi_\theta(a_\tau | o_\tau) \right] \\
&= \mathbb{E}^{\pi^\theta} \left[\sum_{\tau=0}^{+\infty} \sum_{h=\tau}^{+\infty} \gamma^h r_h(o_h, a_h) \nabla_\theta \ln \pi_\theta(a_\tau | o_\tau) \right] \quad // \text{ Change summation order} \\
&= \mathbb{E}^{\pi^\theta} \left[\sum_{\tau=0}^{+\infty} \gamma^\tau \nabla_\theta \ln \pi_\theta(a_\tau | o_\tau) \sum_{h=\tau}^{+\infty} \gamma^{h-\tau} r_h(o_h, a_h) \right] \\
&= \mathbb{E}^{\pi^\theta} \left[\sum_{\tau=0}^{+\infty} \gamma^\tau \nabla_\theta \ln \pi_\theta(a_\tau | o_\tau) \mathbb{E} \left[\sum_{h=\tau}^{+\infty} \gamma^{h-\tau} r_h(o_h, a_h) \mid a_\tau, o_\tau \right] \right] \\
&= \mathbb{E}^{\pi^\theta} \left[\sum_{\tau=0}^{+\infty} \gamma^\tau Q_\tau^{\pi^\theta}(o_\tau, a_\tau) \nabla_\theta \ln \pi_\theta(a_\tau | o_\tau) \right] \quad // \text{ Definition in Eq. (13)} \\
&= \mathbb{E}^{\pi^\theta} \left[\sum_{\tau=0}^{+\infty} \gamma^\tau Q_\tau^{\pi^\theta}(o_\tau, a_\tau) \nabla_\theta \ln \pi_\theta(a_\tau | o_\tau) \right] - \underbrace{\sum_{\tau=0}^{+\infty} \frac{\gamma^\tau V^{\pi^\theta}}{\pi_\theta(a_\tau | o_\tau)} \nabla_\theta \int_{\mathcal{A}} da_\tau \pi_\theta(a_\tau | o_\tau)}_{=0} \\
&= \mathbb{E}^{\pi^\theta} \left[\sum_{\tau=0}^{+\infty} \gamma^\tau A_\tau^{\pi^\theta}(o_\tau, a_\tau) \nabla_\theta \ln \pi_\theta(a_\tau | o_\tau) \right] \quad // \text{ Definition in Eq. (13)}
\end{aligned}$$

where (i) is due to the Markov property:

$$\begin{aligned}
&\nabla_\theta \ln p(o_{1:t}, a_{1:t} | \pi^\theta) \\
&= \nabla_\theta (\ln (\rho(s_1) \cdot \mathbb{O}_1(o_1 | s_1) \cdot \pi_\theta(a_1 | o_1) \cdot \mathbb{T}_h(s_2 | s_1, a_1) \cdot \dots \cdot \mathbb{O}_h(o_h | a_h) \cdot \pi_\theta(a_h | o_h))) \quad (15) \\
&= \nabla_\theta \ln \pi_\theta(a_1 | o_1) + \nabla_\theta \ln \pi_\theta(a_2 | o_2) + \dots + \nabla_\theta \ln \pi_\theta(a_t | o_t)
\end{aligned}$$

□

Next, we extend Theorem 1 in [40] and study the case when the action is generated via a Markov Process. The action probability is expressed by

$$\begin{aligned}
\pi_\theta(a_h | o_h) &= \int_{\mathcal{A}^K} da_h^0 da_h^1 \dots da_h^{K-1} \pi_\theta(a_h^0, a_h^1, \dots, a_h^K | o_h) \\
&= \int_{\mathcal{A}^K} da_h^0 da_h^1 \dots da_h^{K-1} \pi_\theta(a_h^0 | o_h) \cdot \prod_{k=0}^{K-1} \pi_\theta(a_h^{k+1} | a_h^k, o_h) \quad (16)
\end{aligned}$$

where we write $a_h = a_h^K$. Bringing Eq. (16) to Eq. (14), we obtain

$$\begin{aligned}
& \nabla_\theta J(\pi^\theta) \\
&= \mathbb{E}^{\pi^\theta} \left[\sum_{\tau=0}^{+\infty} \gamma^\tau A_\tau^{\pi^\theta}(o_\tau, a_\tau) \nabla_\theta \ln \pi_\theta(a_\tau | o_\tau) \right] \\
&= \sum_{\tau=0}^{+\infty} \gamma^\tau \int_{\mathcal{A}} da_\tau \cancel{\pi_\theta(a_\tau | o_\tau)} A_\tau^{\pi^\theta}(o_\tau, a_\tau) \frac{1}{\cancel{\pi_\theta(a_\tau | o_\tau)}} \nabla_\theta \pi_\theta(a_\tau | o_\tau) \\
&= \sum_{\tau=0}^{+\infty} \gamma^\tau \int_{\mathcal{A}} da_\tau^K A_\tau^{\pi^\theta}(o_\tau, a_\tau) \cdot \left[\int_{\mathcal{A}^K} da_\tau^0 da_\tau^1 \dots da_\tau^{K-1} \nabla_\theta \left(\pi_\theta(a_\tau^0 | o_\tau) \cdot \prod_{t=0}^{K-1} \pi_\theta(a_\tau^{t+1} | a_\tau^t, o_\tau) \right) \right] \\
&= \sum_{\tau=0}^{+\infty} \gamma^\tau \int_{\mathcal{A}^{K+1}} da_\tau^0 \dots da_\tau^K \cdot A_\tau^{\pi^\theta}(o_\tau, a_\tau) \cdot [\nabla_\theta \exp \ln \pi_\theta(a_\tau^0, a_\tau^1, \dots, a_\tau^K | o_\tau)] \\
&= \sum_{\tau=0}^{+\infty} \gamma^\tau \int_{\mathcal{A}^{K+1}} da_\tau^0 \dots da_\tau^K \cdot A_\tau^{\pi^\theta}(o_\tau, a_\tau) \cdot [\pi_\theta(a_\tau^0, a_\tau^1, \dots, a_\tau^K | o_\tau) \cdot \nabla_\theta \ln \pi_\theta(a_\tau^0, a_\tau^1, \dots, a_\tau^K | o_\tau)] \\
&= \mathbb{E}^{\pi^\theta} \left[\sum_{\tau=0}^{+\infty} \gamma^\tau A_\tau^{\pi^\theta}(o_\tau, a_\tau) \nabla_\theta \ln \pi_\theta(a_\tau^0, a_\tau^1, \dots, a_\tau^K | o_\tau) \right] \\
&= \mathbb{E}^{\pi^\theta} \left[\sum_{\tau=0}^{+\infty} \gamma^\tau A_\tau^{\pi^\theta}(o_\tau, a_\tau) \nabla_\theta \sum_{k=0}^{K-1} \ln \pi_\theta(a_\tau^{k+1} | a_\tau^k, o_\tau) \right]
\end{aligned} \tag{17}$$

In what follows, we consider the case where the POMDP has stationary transition kernels, and the policy is reactivative and stationary. This setting makes A^π, Q^π, V^π time independent, so we drop their subscripts h for brevity:

$$\nabla_\theta J(\pi^\theta) = \mathbb{E}_{o, a^0, a^1, \dots, a^K}^{\pi^\theta} \left[\sum_{\tau=0}^{+\infty} \gamma^\tau A^{\pi^\theta}(o, a^K) \nabla_\theta \sum_{k=0}^{K-1} \ln \pi_\theta(a^{k+1} | a^k, o) \right] \tag{18}$$

To proceed from the RHS of Eq. (18), we first show that for any function $f(\cdot, \cdot) : \mathcal{O} \times \mathcal{A} \rightarrow \mathbb{R}$ and a reactive, stationary policy π , the following relation holds:

$$\mathbb{E}^\pi \left[\sum_{h=0}^{+\infty} \gamma^h f(o_h, a_h) \right] = \frac{1}{1-\gamma} \mathbb{E}_{o \sim d_\rho^\pi(\cdot)} [\mathbb{E}_{a \sim \pi(\cdot | o)} [f(o, a)]] \tag{19}$$

where we take the expectation of observation o with respect $d_\rho^\pi(o)$, the discounted average visitation frequency to that observation given initial state distribution. Concretely speaking, $d_\rho^\pi(o)$, which we call the “observation visitation measure”, is defined by

$$d_{s_1}^\pi(o) := (1-\gamma) \sum_{h=0}^{+\infty} \gamma^h \int_{\mathcal{O}} do p(o_h = o | s_1; \pi) \tag{20a}$$

$$d_\rho^\pi(o) := \mathbb{E}_{s_1 \sim \rho(\cdot)} [d_{s_1}^\pi(o)] \tag{20b}$$

The MDP version for this result can be found in classical RL theory textbooks, such as Eq. (0.10) on page 27 of [1]. Below, we extend the MDP result to POMDPs.

Proof.

$$\begin{aligned}
\text{LHS} &= \int_S ds_1 \rho(s_1) \sum_{h=0}^{+\infty} \gamma^h \int_{\mathcal{O} \times \mathcal{A}} do_h da_h p(o_h, a_h | s_1) f(o_h, a_h) \\
&= \int_S ds_1 \rho(s_1) \sum_{h=0}^{+\infty} \gamma^h \int_{\mathcal{O} \times \mathcal{A}} do_h da_h p(o_h | s_1) \pi_h(a_h | o_h) f(o_h, a_h) \\
&= \frac{1}{1-\gamma} \int_S ds_1 \rho(s_1) (1-\gamma) \sum_{h=0}^{+\infty} \gamma^h \int_{\mathcal{O}} do_h p(o_h | s_1) \int_{\mathcal{A}} da_h \pi_h(a_h | o_h) f(o_h, a_h) \\
&= \frac{1}{1-\gamma} \mathbb{E}_{s_1 \sim \rho(\cdot)} (1-\gamma) \sum_{h=0}^{+\infty} \gamma^h \int_{\mathcal{O}} do p(o_h = o | s_1) \mathbb{E}_{a \sim \pi_h(\cdot | o_h)} f(o, a) \quad // \text{Re-labeling} \\
&:= \frac{1}{1-\gamma} \mathbb{E}_{s_1 \sim \rho(\cdot)} \mathbb{E}_{o \sim d_{s_1}(\cdot)} \mathbb{E}_{a \sim \pi_h(\cdot | o_h)} f(o, a) \quad // \text{Eq. (20a)} \\
&:= \frac{1}{1-\gamma} \mathbb{E}_{o \sim d_\rho(\cdot)} \mathbb{E}_{a \sim \pi_h(\cdot | o_h)} f(o, a) \quad // \text{Eq. (20b)} \\
&= \frac{1}{1-\gamma} \mathbb{E}_{o \sim d_\rho(\cdot)} \mathbb{E}_{a \sim \pi(\cdot | o)} f(o, a) \quad // \text{Stationary Policy}
\end{aligned}$$

□

Instantiate the function f in Eq. (19) as the product of the advantage function times and the gradient of the joint log probability, we arrive at the following result by plugging Eq. (19) into Eq. (18):

$$\nabla_\theta J(\pi^\theta) = \frac{1}{1-\gamma} \mathbb{E}_{o \sim d_\rho^\theta(\cdot)} \mathbb{E}_{a^0, a^1, \dots, a^K \sim \pi^\theta(\cdot | o)} \left[A^{\pi^\theta}(o, a) \nabla_\theta \sum_{k=0}^{K-1} \ln \pi_\theta(a^{k+1} | a^k, o) \right] \quad (21)$$

where a stands for a^K . We take the expectation of observation concerning its visitation measure and the expectation of intermediate actions for the distribution induced by the policy's Markov Process.

We remind the reader that Eq. (21) holds only for POMDPs with a stationary and reactive policy.

A.2 Action Chunking

In practice, we implement a flow matching policy with action chunking, which slightly alters how we compute the policy's log probability. Our robots interact with the environment in a manner similar to Diffusion Policy [12], where the agent receives one observation, outputs a sequence of actions, executes each action, collects rewards per step, and accumulates them for optimization.

This interaction protocol implies that actions in a chunk are fixed after the first observation and remain unaffected by later observations that may change during execution. Thus, actions within a chunk are conditionally independent, given the initial observation. In our setup, we flatten the actions of the chunk into a single vector as the actor's output, ensuring that the actions in the chunk are independent given the network's inputs, which include the action chunk at the last denoising step, the observation, and the denoising time. Hence, the log probability of a chunk of size C is the sum of the log probabilities of its internal actions. Formally:

$$\begin{aligned}
&\ln \pi_{\bar{\theta}}(a_{h:h+C-1}^{k+1} | t_k, a_{h:h+C-1}^k, o_h) \\
&= \sum_{c=0}^{C-1} \ln \pi_{\bar{\theta}}(a_{h+c}^{k+1} | t_k, a_{h:h+C-1}^k, o_h) \quad // \text{Conditional Independence} \\
&= \sum_{c=0}^{C-1} \ln \mathcal{N}\left(a_{h+c}^{k+1} \left| a_{h+c}^k + [v_\theta]_{h+c} \cdot \Delta t_k, [\sigma_{\theta'}]_{h+c}^2 \right.\right)
\end{aligned} \quad (22)$$

In Eq. (22), the terms v_θ and $\sigma_{\theta'}$ are conditioned on $(t_k, a_{h:h+C-1}^k, o_h)$. We use $[u]_i$ to denote the i -th element of vector u , and $u_{i:j}$ to represent the sub-vector formed by concatenating the i -th to the j -th coordinates of u .

B Extended Related Work

Diffusion Policy Policy Optimization [42] Diffusion Policy Policy Optimization (DPPO) trains DDIM policies with PPO. They design the algorithm on top of a bi-level MDP formulation, which involves calculating the advantage function for the denoised actions.

$$\mathcal{L}_\theta = \mathbb{E} \min \left(\hat{A}^{\pi_{\theta_{\text{old}}}}(\bar{s}_{\bar{t}}, \bar{a}_{\bar{t}}) \frac{\bar{\pi}_\theta(\bar{s}_{\bar{t}}, \bar{a}_{\bar{t}})}{\bar{\pi}_{\theta_{\text{old}}}(\bar{s}_{\bar{t}}, \bar{a}_{\bar{t}})}, \hat{A}^{\pi_{\theta_{\text{old}}}}(\bar{s}_{\bar{t}}, \bar{a}_{\bar{t}}) \text{clip} \left(\frac{\bar{\pi}_\theta(\bar{s}_{\bar{t}}, \bar{a}_{\bar{t}})}{\bar{\pi}_{\theta_{\text{old}}}(\bar{s}_{\bar{t}}, \bar{a}_{\bar{t}})}, 1 - \varepsilon, 1 + \varepsilon \right) \right) \quad (23)$$

The term $\bar{t} = \bar{t}(t, k)$ represents the k -th denoising step in the t -th interaction. They define the advantage function at these denoising steps by applying an additional discount factor, $\gamma_{\text{denoise}}^k$, to the advantage function of the action taken.

DPPO does not provide a theoretical guarantee for its design in Eq. (23). Computing the advantage function at denoised steps also slows down computation. Our method does not perform such calculations, and we derive our algorithm from rigorous reinforcement learning theory for POMDPs elaborated in Appendix A.

Empirically, Section 5 shows our method, ReinFlow, outperforms DPPO in almost all tasks in Gym and Franka Kitchen while reducing the denoising step count from 10 in DPPO to 4 in ReinFlow, significantly reducing wall time as shown in Table 3. Shortcut Model policies trained in visual manipulation tasks achieved a comparable or slightly better success rate than DPPO, using as few as one step in Can and Square and four steps in Transport. DDIM policies in DPPO adopt five steps for these tasks.

Flow Q Learning [38] Flow Q Learning (FQL) is an offline reinforcement learning algorithm designed for flow matching policies, which can also be used for offline-to-online fine-tuning.

Unlike our approach, FQL does not directly fine-tune a flow model with multiple denoising steps. Instead, it first trains a multi-step flow policy π_θ using the objective in Eq. (2). Then, it learns a Q function Q_ϕ from an offline RL dataset using one-step temporal difference (TD) learning, as described in [51].

$$\mathcal{L}(\phi) := \mathbb{E} \left[\left(Q_\phi(s, a) - r - \gamma Q_\phi(s', \pi_\omega(s', z)) \right)^2 \right] \quad (24)$$

At the same time, FQL distills a one-step policy π_ω from the pre-trained flow via minimizing the following loss:

$$\mathcal{L}(\omega) := \mathbb{E} \left[-Q_\phi(s, \mu_\omega(s, z)) + \alpha \|\mu_\omega(s, z) - \mu_\theta(s, z)\|_2^2 \right] \quad (25)$$

The one-step policy will be deployed after FQL fine-tuning.

In the official FQL implementation, gradients flow to the multi-step policy during the distillation of the one-step policy, which can interfere with the pre-trained loss. As a result, we discover that even when we align the sample consumption during the offline RL phase, the multi-step FQL policy may struggle to match the reward achieved by pure behavior cloning pre-training.

In contrast, ReinFlow’s method directly and stably fine-tunes a multi-step flow matching policy, offering richer representation capabilities than one-step distilled models in FQL. Empirically, ReinFlow outperforms FQL asymptotically and converges faster regarding wall-clock time, as shown in Figures 1 and 2. Additionally, ReinFlow does not rely on distillation. As a purely online RL algorithm, ReinFlow does not require labeled rewards for expert demonstrations.

Other Methods DPPO [42] and FQL [38] provided an excellent introduction to a line of algorithms that fine-tune diffusion models with online RL and flow models with offline RL, including IDQL [23], QSM [40], DAWR [42], DIPO [55], DRWR [42], DQL [54], IFQL [38], etc. DPPO and FQL are generally superior to these methods regarding asymptotic reward, training stability, and wall time.

Although we have shown the advantage of ReinFlow over DPPO and FQL in Section 5, for completeness, we provide a brief comparison between the diffusion RL baselines with our method in a few representative continuous control tasks with the same set of hyperparameters indicated in [42]. Please refer to Appendix E for details.

C Environment and Dataset Configuration

Tasks. Figures 8 and 9 demonstrate the locomotion and manipulation tasks considered in this work.

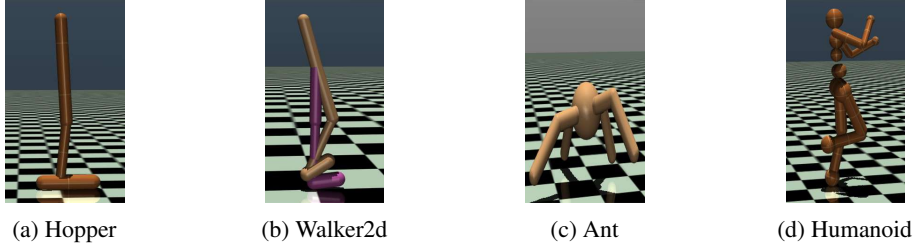


Figure 8: Four OpenAI Gym locomotion Tasks: Hopper, Walker2d, Ant, and Humanoid.

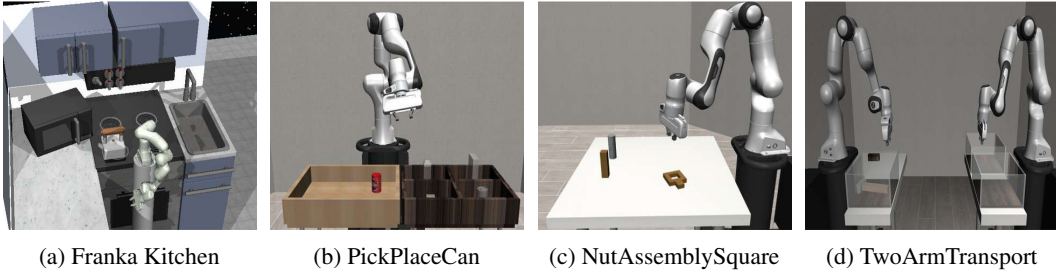


Figure 9: Four manipulation tasks in state-input Franka Kitchen and pixel-input Robomimic environments.

Environment Configuration. We also list the environment configurations in different tasks in Table 1.

Table 1: Environment Configuration

Environment	Task or Dataset	State Dim	Image Shape	Action Chunk	Max. Eps. Len. H	Reward
OpenAI Gym	Hopper-v2	11	-	3×4	1000	Dense
	Walker2d-v2	17	-	6×4	1000	Dense
	Ant-v0	111	-	8×4	1000	Dense
	Humanoid-v3	376	-	17×4	1000	Dense
Franka Kitchen	Kitchen-Complete-v0	60	-	9×4	280	Sparse
	Kitchen-Mixed-v0	60	-	9×4	280	Sparse
	Kitchen-Partial-v0	60	-	9×4	280	Sparse
Robomimic	Can	9	$[3,96,96] \times 1$	7×4	300	Sparse
	Square	9	$[3,96,96] \times 1$	7×4	400	Sparse
	Transport	18	$[3,96,96] \times 2$	14×8	800	Sparse

In Tab. 1, the “State Dim” indicates the dimension of proprioception inputs. “Action Chunk” expresses the dimension of a single action and the size of the action chunk. “Max.Eps.Len. H ” indicates the maximum steps a robot can take in a single rollout. When the reward is “sparse, we award the agent a reward of +1 only upon task completion. Otherwise, the agent receives a 0 reward. The sparse reward is realistic, straightforward, and directly associated with the success rate of manipulation tasks. A “dense” reward system assigns the reward based on the robot’s dynamics and kinematic properties. It is usually a floating number after each step of action execution. Dense reward systems need careful design. We adopt them primarily in sim2real training for legged locomotion tasks.

The Robomimic Dataset Provided by DPPO [42] We remark that, in Robomimic environments, we adhere to the configuration of DPPO [42], which makes the shapes of the state vector smaller than the official default implementation in [36]. This processing simplifies robot learning and makes the pre-trained data provided by [42] smaller and simpler than Robomimic’s official datasets. As acknowledged by the authors of DPPO, the datasets provided by [42] are of lower quality and/or quantity than the official release, so the pre-trained policy is trained on inferior data. Consequently, the pre-trained checkpoints of both DDPM and Shortcut policies have a lower success rate than the best-reported results in the literature [18].

We can train flow matching or diffusion policies with RoboMimic’s default configuration and datasets, which will help us align with state-of-the-art results in the imitation learning literature. However, we may need to adopt larger neural networks and spend more time pre-training and fine-tuning.

Datasets for OpenAI Gym Tasks To faithfully replicate the results of DPPO [42], we trained both DPPO and ReinFlow agents using the behavior cloning (BC) dataset provided by Ren et al. (2024) [42]. For consistency, we followed their dataset choices for all experiments in the Appendix that do not involve offline reinforcement learning (RL) algorithms, such as FQL.

However, the DPPO dataset for OpenAI Gym tasks lacks the offline rewards necessary to train an FQL agent, and the authors did not specify how they constructed their Gym dataset. We hypothesize that their BC datasets were derived and augmented from D4RL [19]. Therefore, in the experiments that involve FQL (described in Section 5.2 of the main text), we adopted D4RL offline RL datasets to train DPPO, FQL, and ReinFlow agents. We also remark that while we chose the “Ant-v2” environment in these experiments, we switched to “Ant-v0” in the sensitivity analysis in Section 4.3 and the Appendix.

The minor differences in OpenAI Gym Tasks mentioned above resulted in minimal discrepancy in reward curves.

D Implementation Details

D.1 Model Architecture

For a fair comparison, we try to make the model architecture of flow matching policies align with diffusion policies proposed in DPPO [42] as much as possible.

State-input Tasks. In state-input tasks (OpenAI Gym and Franka Kitchen), the velocity nets v_θ of 1-ReFlow policies are parameterized with Multi-layer Perceptrons (MLP) that receive action chunk, state, and time features. The time input $t \in (0, 1)$ is encoded by sinusoidal positional embedding [25] and linear projections, with a Mish [37] activation function in between. We implement Shortcut Models similarly, passing the time and inference step counts through the same sinusoidal positional embedding and concatenating. At the same time, we also encode the state input with a small MLP and add the state feature with the time-step features. The sizes of Shortcut Models are often slightly smaller than 1-ReFlow policies in the same task. Critic networks are also MLPs with the same or half the width.

Pixel-input Tasks. In Robomimic, where the agent receives pixel and proprioception inputs, the actor and the critic adopt a single-layer Visual Transformer [15] with random shift augmentation as the visual encoder and compresses the proprioception information with a small MLP. We pass the features of the visuomotor condition, time embedding, and the raw action chunk through the actor’s velocity head, which outputs a velocity estimate. The critic only receives features from time and condition.

Noise Injection Net The noise injection network θ' shares the input features with the actor and outputs the standard deviation of the noise at each coordinate of the actions in the action chunk. The output of network θ' is passed through a Tanh function coupled with affine transform, to ensure bounded output and smooth gradients. The upper and lower bounds of the noise standard deviation $\sigma_{\max}, \sigma_{\min}$ are a group of essential hyperparameters of ReinFlow, and we have provided an analysis in Section 6 to study how they influence exploration.

We discard $\sigma_{\theta'}$ after fine-tuning. Although a noise-injected process exists during RL, ReinFlow still returns a policy with an ODE inference path.

During the evaluation, we also did not inject noise into the flow policy; We observed that the reward is often higher than the noise-injected version, aligning with findings in classical RL literature [22].

Parameter Scale We summarize the sizes of the actor, critic, and noise injection networks in Table 2, which shows that for state-input tasks, a negligible parameter increase ($< 6\%$) brought by the noise injection network returns promises a 135.36% net increase in reward and a 31.29% net increase in success rate.

For complex visual manipulation tasks beyond robomimic, since the noise network θ' shares the same representation backbone as the velocity network, the parameter increase should also remain minimal when scaling to larger models with more complex backbones, such as multi-layer Transformers, instead of the single-layer Transformer used in our experiments.

Designing an efficient noise injection network architecture that balances reward improvement and parameter count is an interesting problem, which we leave for future work.

Table 2: Model Parameter Counts

Task	Model	Pre-trained Actor θ /M	Noise Net θ' /M	Fine-tuned Actor $\bar{\theta}$ /M	Critic /M	Total /M	Noise/ Velocity
Hopper-v2	1-ReFlow	0.55	0.01	0.56	0.13	0.69	1.22%
Walker2d-v2	1-ReFlow	0.57	0.01	0.58	0.14	0.71	1.39%
Ant-v3	1-ReFlow	0.62	0.01	0.64	0.16	0.80	2.31%
Humanoid-v3	1-ReFlow	0.80	0.03	0.83	0.23	1.06	4.23%
Kitchen	Shortcut	0.16	0.01	0.17	0.15	0.31	5.46%
Can	Shortcut	1.01	0.15	1.16	0.59	1.74	14.59%
Square	Shortcut	1.69	0.32	2.01	0.59	2.59	18.91%
Transport	Shortcut	1.87	0.35	2.22	0.66	2.87	18.84%

D.2 Enhancing Training Stability

Clipping Probability Ratio For stability reasons, we clip the log probability ratio in Algorithm 1 with $\epsilon = 0.01$ for state-input tasks and $\epsilon = 0.001$ for pixel-input tasks. This choice follows DPPO [42].

Clipping Denoised Actions Although unnecessary for the pre-trained flow policies, we discover that during fine-tuning, it is beneficial to clip the denoised actions of a flow matching policy because this helps prevent the injected noise from interrupting the integration path too violently. After fine-tuning with ReinFlow, policies should also clip the denoised actions during inference; otherwise, performance may likely deteriorate.

Critic Warmup Training the critic network for several iterations before updating the actor is crucial for stable training and rapid convergence, particularly for larger models with visual inputs. We refer to this phase as “critic warm-up”. Since we use RL as a fine-tuning approach, the critic should output a reasonably large value (at least positive) before the policy gradient starts. An excessively small or even negative initial output misleads the actor into considering its current actions as excessively unsatisfying, resulting in rapidly degrading rewards and value function estimates during the fine-tuning process.

Empirically, we recommend initializing the critic and/or adjusting the critic warm-up iteration number according to the initial reward of the pre-trained policy, the rollout step number, and the discount factor.

Critic Overfitting and Initialization An excessively long warm-up period may lead to overfitting of the critic network, especially in cases where the critic is significantly smaller than the pre-trained policy (Table 2). When the critic overfits, the policy gradient loss could oscillate violently during fine-tuning.

One possible solution to address critic overfitting is to incorporate regularizations into the critic’s training procedure. Another method is to limit the warm-up iterations and initialize the critic’s last fully connected layer with a positive bias. The bias can be estimated by the pre-trained success rate. With a positive initial output, the critic requires fewer warm-up iterations to output an appropriate value estimate without overfitting the pre-trained policy’s distributions.

E Additional Experimental Results

Random seeds Unless specified, we train all the RL algorithms with three seeds for all tasks except for Franka Kitchen with mixed or partial data, where we adopt two extra seeds, in the main experiment section 5. These tasks involve long-horizon multi-task planning, and we discover that DPPO and ReinFlow exhibit high variations across different runs.

The RL fine-tuning curves show the reward or success rate averaged over these seeds, with shading representing the mean \pm standard deviation to indicate variability across runs.

Rendering Backend During training and wall time testing, the MuJoCo graphics rendering backend (MUJOCO_GL) is set to Embedded System Graphics Library (EGL) to accelerate the computation with GPU. If users do not have EGL support and they switch to software rendering (osmesa), or if multiple threads are running together on the same group of CPU kernels or the same GPU, the compute time may be longer than that described in Table 3.

Table 3: Per Iteration Wall-clock Time

Task	Algorithm	Single Iteration Time/second			Average
		First seed	Second seed	Third seed	Mean \pm Std
Hopper-v2	ReinFlow-R	11.598	11.704	11.843	11.715 ± 0.123
	ReinFlow-S	12.051	12.127	12.372	12.290 ± 0.141
	DPPO	99.502	99.616	98.021	99.046 ± 0.890
	FQL	4.373	4.366	4.515	4.418 ± 0.084
Walker2d-v2	ReinFlow-R	11.861	11.446	11.382	11.563 ± 0.260
	ReinFlow-S	12.393	12.690	13.975	13.019 ± 0.841
	DPPO	101.151	106.125	98.470	101.915 ± 3.884
	FQL	5.248	4.597	5.207	5.017 ± 0.365
Ant-v0	ReinFlow-R	17.210	17.685	17.524	17.473 ± 0.242
	ReinFlow-S	17.291	17.821	18.090	17.734 ± 0.407
	DPPO	102.362	104.632	99.042	102.012 ± 2.811
	FQL	5.242	4.950	5.3086	5.167 ± 0.191
Humanoid-v3	ReinFlow-R	31.437	30.223	31.088	30.916 ± 0.625
	ReinFlow-S	30.499	30.058	31.029	30.529 ± 0.486
	DPPO	109.884	105.455	113.358	109.566 ± 3.961
	FQL	5.245	4.981	5.522	5.249 ± 0.271
Franka Kitchen	ReinFlow-S	26.655	26.328	26.628	26.537 ± 0.182
	DPPO	81.584	84.646	83.245	83.158 ± 1.533
	FQL	5.245	4.981	5.522	5.249 ± 0.271
Can (image)	ReinFlow-S	219.943	216.529	217.711	218.061 ± 1.734
	DPPO	310.974	307.811	308.014	308.933 ± 1.771
Square (image)	ReinFlow-S	313.457	312.3	313.862	313.206 ± 0.811
	DPPO	438.506	440.212	434.773	437.830 ± 2.782
Transport (image)	ReinFlow-S	554.196	557.712	559.006	558.359 ± 0.915
	DPPO	406.607	439.268	412.077	419.317 ± 17.493

Wall-clock Time For a fair comparison, we measure all algorithms’ wall-clock time in all the tasks (except Transport) on a single NVIDIA RTX 3090 GPU with EGL rendering. We evaluate the wall time of Robomimic Transport on two NVIDIA A100 GPUs with EGL rendering, as this task occupies significantly more memory than a single RTX 3090 GPU. The measurement is taken sequentially for three random seeds without interfering with other processes. We obtain the total wall-clock time for each algorithm by multiplying the average iteration time by the number of iterations. Table 3 provides a detailed record of these measurements, where the results are recorded in seconds and accurate to three decimal places.

Although FQL’s per-iteration wall time is significantly shorter than other methods, this does not imply that it is more efficient overall: FQL’s batch size is considerably smaller than that of PPO-based methods, including ReinFlow and DPPO, and its total training iterations are significantly larger than those of the other two methods; neither is FQL designed for parallel computing like DPPO and ReinFlow.

Performance Increase We report the performance improvement after fine-tuning flow matching policies with ReinFlow across various simulation tasks in Table 4.

For locomotion tasks, we compute the reward increase ratio as follows:

$$\text{Locomotion Reward Net Increase Ratio} := \frac{\text{Fine-tuned Reward} - \text{Pre-trained Reward}}{\text{Pre-trained Reward}} \quad (26)$$

For manipulation tasks, we compute the success rate increase:

$$\text{Manipulation Success Rate Net Increase} := \text{Fine-tuned Success Rate} - \text{Pre-trained Success Rate} \quad (27)$$

Policies fine-tuned with ReinFlow achieved an average episode reward net increase of **135.36%** in OpenAI Gym locomotion tasks using D4RL datasets, with an average success rate increase of **31.29%** in Franka Kitchen, **45.77%** in Robomimic, and **40.34%** in all manipulation tasks. The results are accurate to two decimal places.

Sample Complexity in Gym Tasks Here, we also compare the sample complexity in OpenAI Gym tasks omitted in the main text. While FQL is more sample efficient in simpler tasks such as Hopper and Walker2d, it generally struggles to tackle more complex locomotion task, where it is asymptotically inferior to DPPO and ReinFlow.

Comparison with Other Diffusion RL Methods We compare the diffusion RL baselines with our method in a few representative continuous control tasks. For these baselines, we adopt the same set of hyperparameters described in [42].

Figs 11 and 12 show that ReinFlow overall outperforms other methods concerning the stability w.r.t random seeds and asymptotic performance.

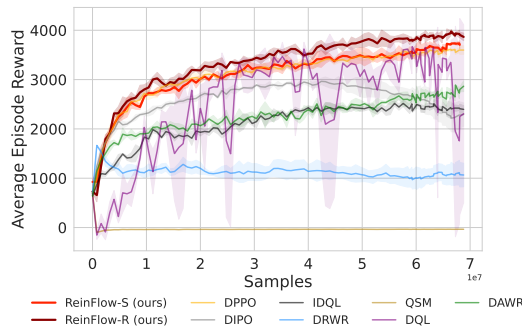


Figure 11: Fine-tuning locomotion task Ant-v0 with Diffusion RL baselines and ReinFlow.

Table 4: Performance Metrics for ReinFlow Across Tasks.

(a) Average Episode Reward in Locomotion Tasks.

Task	Algorithm	Pre-trained Episode Reward	Fine-tuned Episode Reward	Reward Net Increase Ratio
Hopper-v2	ReinFlow-R	1431.80 \pm 27.57	3205.33 \pm 32.09	123.87%
	ReinFlow-S	1528.34 \pm 14.91	3283.27 \pm 27.48	114.83%
Walker2d-v2	ReinFlow-R	2739.90 \pm 74.57	4108.57 \pm 51.77	49.95%
	ReinFlow-S	2739.19 \pm 134.30	4254.87 \pm 56.56	55.33%
Ant-v2	ReinFlow-R	1230.54 \pm 8.18	4009.18 \pm 44.60	225.81%
	ReinFlow-S	2088.06 \pm 79.34	4106.31 \pm 79.45	225.81%
Humanoid-v3	ReinFlow-R	1926.48 \pm 41.48	5076.12 \pm 37.47	163.49%
	ReinFlow-S	2122.03 \pm 105.01	4748.55 \pm 70.71	123.77%

(b) Average Success Rate in Manipulation Tasks.

Environment and Task	Algorithm	Pre-trained Success Rate	Fine-tuned Success Rate	Success Rate Net Increase
Kitchen-complete	ReinFlow-S	73.16 \pm 0.84%	96.17 \pm 3.65%	23.01%
Kitchen-mixed	ReinFlow-S	48.37 \pm 0.78%	74.63 \pm 0.36%	26.26%
Kitchen-partial	ReinFlow-S	40.00 \pm 0.28%	84.59 \pm 12.38%	44.59%
Can (image)	ReinFlow-R	59.00 \pm 3.08%	98.67 \pm 0.47%	39.67%
	ReinFlow-S	57.83 \pm 1.25%	98.50 \pm 0.71%	40.67%
Square (image)	ReinFlow-R	25.00 \pm 1.47%	74.83 \pm 0.24%	49.83%
	ReinFlow-S	34.50 \pm 1.22%	74.67 \pm 2.66%	40.17%
Transport (image)	ReinFlow-S	30.17 \pm 2.46%	88.67 \pm 4.40%	58.50%

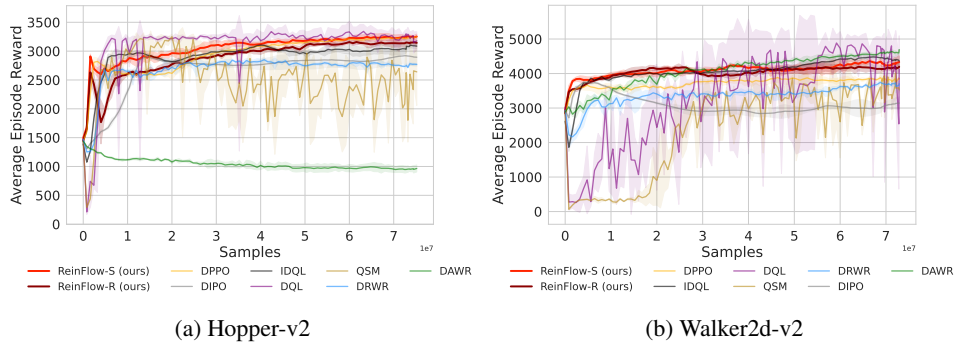


Figure 12: Fine-tuning locomotion task Hopper-v2 and Walker2d-v2 with Diffusion RL baselines and ReinFlow.

Changing the Behavior Cloning Dataset’s Scale in Square Tab. 5 shows how the fine-tuned performance of ReinFlow is affected by the scale of the behavior cloning dataset in robomimic square. Fine-tuning the policy trained on 16 episodes failed due to an overly low initial success rate. We adopt the same hyperparameter set when fine-tuning policies trained on 64 and 100 episodes, restricting the

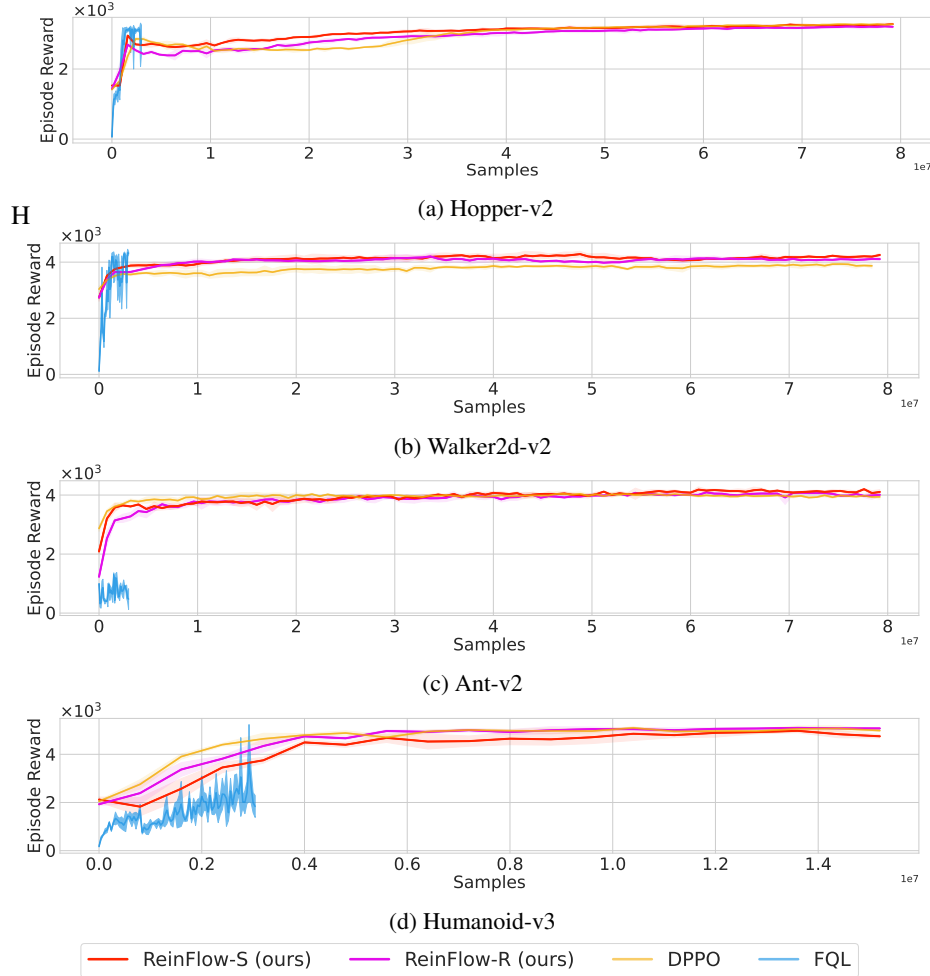


Figure 10: Sample efficiency results of state-based locomotion tasks in OpenAI Gym. For better visualization, we down-sampled FQL’s data by five times in the first three tasks and three times in “Humanoid-v3”. Although FQL is more sample-efficient than DPPO and ReinFlow in simpler tasks, it struggles to achieve high reward in more challenging locomotion tasks.

noise standard deviation to $\text{std} \in [0.08, 0.14]$ with entropy coefficient 0.01. We slightly tuned down the noise to $\text{std} \in [0.06, 0.10]$ and removed entropy regularization, as we find it is more beneficial to limit exploration when the pre-trained policy performs poorly.

Table 5: Fine-tuned Success Rates in Square Across Different Pre-trained Episodes

Pre-trained Episodes	Pre-trained Success Rate	Fine-tuned Success Rate			Average Fine-tuned Success Rate	
		Fist seed	Second seed	Third seed	Mean	Std
16	3.08 %	0.00 %	0.00 %	0.00 %	3.08 %	0.00 %
32	10.15%	22.20%	22.00%	18.50%	20.90%	1.70 %
64	27.67%	65.50%	62.20%	56.20%	61.30%	3.85 %
100	25.14%	79.50%	78.20%	74.50%	77.40%	2.12 %

Changing the Number of Fine-tuned Denoising Steps Altering the fine-tuned denoising step number K could affect ReinFlow’s performance since the pre-trained policy has different rewards when evaluated at different steps.

Fig. 13 shows the difference when fine-tuning a Shortcut Policy in Franka Kitchen at $K = 1, 2$, and 4 denoising steps.

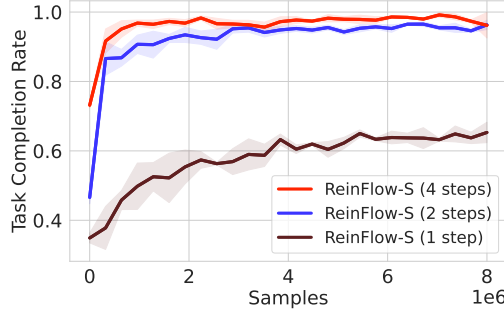


Figure 13: Fine-tuning Shortcut Policy in Kitchen-complete-v0 at Different Denoising Steps 1, 2, and 4.

In Fig. 13, all the run hyperparameters except K and random seeds are the same. The pre-trained policy adopts complete demonstration data.

Increasing K improves the reward at the beginning of fine-tuning. A better starting point shrinks the space of exploration and thus accelerates convergence. However, a longer denoising trajectory also consumes more simulation time. Fig. 13 and Fig. 4a also show that the success rate or episode reward quickly plateaus when scaling K .

In more challenging tasks such as visual manipulation, we also find that reducing the noise standard deviation is beneficial when we increase the number of denoising steps K , especially when the pre-trained policy has a low success rate.

F Discussion

In this section we provide additional discussion to help the readers better understand our design.

F.1 Noise Injection versus Entropy Regularization

Both noise injection and entropy regularization serve to enhance exploration in reinforcement learning, but they play distinct and complementary roles in ReinFlow.

Purpose and mechanism. Noise injection is primarily used to replace the $\log \pi$ function, making the action distribution tractable. The added stochasticity naturally aids exploration as a byproduct. In contrast, entropy regularization provides an explicit mechanism to control exploration via its coefficient α . The noise network enables ReinFlow to learn diverse actions by adapting noise intensity across denoising steps, while entropy regularization offers direct, tunable control over the exploration-exploitation trade-off. Importantly, ReinFlow remains mathematically valid even without the entropy term.

Generalization beyond locomotion. Entropy regularization is effective across various types of tasks, not only in locomotion domains. We successfully adopt it in the Robomimic visual manipulation task “square” (Table 9b, Appendix). Furthermore, in the “Franka Kitchen-complete” task—a state-input, sparse-reward manipulation environment—entropy regularization yields meaningful improvements in success rate. Ablation experiments averaged over 3 seeds show an increase from $96.17 \pm 3.65\%$ (without regularization of the entropy) to $99.00 \pm 0.75\%$ (with regularization of the entropy, $\alpha = 0.1$).

F.2 Wall-time Efficiency

ReinFlow achieves faster wall-time performance for three key reasons:

(a) Fewer Denoising Steps: Flow models (e.g., ReFlows) require fewer steps than diffusion models (e.g., DDPM, DDIM) to reach high initial reward.

(b) Exact Probability Description in Few Steps: The probability of flow ODEs depends on the number of denoising steps. However, ReinFlow’s expression remains exact even with very few steps, making it possible to take advantage of flow’s property, enabling efficient fine-tuning without compromising reward.

(c) Simplified Optimization: We simplify DPPO’s policy loss by not computing value/ advantage for denoised actions. This further reduces the computational cost.

F.3 Additional Ablation Studies

We conducted additional ablation studies across various tasks during the rebuttal period, confirming that the observed trends are consistent.

Noise conditioning across environments. We compared the effect of different noise conditioning strategies in the Humanoid-v3 environment, conducting experiments with three random seeds. We evaluated conditioning only on state ($\sigma_{\theta'}(s)$) versus conditioning on both state and time ($\sigma_{\theta'}(s, t)$):

Task	$\sigma_{\theta'}(s)$	$\sigma_{\theta'}(s, t)$
Humanoid	4987.39 ± 97.82	5076.12 ± 37.47

These results demonstrate that conditioning the noise on both time and state yields higher rewards, consistent with the findings presented in Fig. 5 (page 9).

Noise scale in sparse-reward manipulation. We trained ReinFlow agents with different noise scales in the Franka Kitchen-complete task, with results averaged over three seeds:

Noise std	Success Rate
0.001	$70.42\% \pm 3.21\%$
0.08	$90.67\% \pm 14.87\%$
0.16	$99.08\% \pm 1.01\%$

This experiment reveals that larger noise levels promote exploration. Together, these additional experiments demonstrate that the design choices and trends identified are robustly generalized across different types of environment, reward structures, and task complexities.

G Reproducing Our Findings

We list the key hyper-parameters and model architectures needed to reproduce the experiment results of ReinFlow and other baseline algorithms.

G.1 Hyperparameters of ReinFlow

We adopt the same batch size suggested in DPPO [42] and follow their implementation to normalize the reward with time-reversed running variance.

It is essential to adjust the number of critic warmup iterations according to the performance of the pre-trained policy. A larger initial reward requires more warmup steps.

We clipped the denoised actions within $[-1, 1]$ to enhance training stability in implementation. Table 7 indicates this option with “clip intermediate actions”. We also find it beneficial to slightly reduce the maximum noise standard deviation in the latter training course to postpone the reward decrease. $\cos(r_1, r_2)$ indicates a learning rate that decays in the rate of a cosine function from r_1 to r_2 .

Table 6: ReinFlow’s Shared Hyperparameters Across All Tasks

Parameter	Value
critic loss coefficient	0.50
GAE lambda λ	0.95
reward scale	1.0
reward normalization	True
actor optimizer	Adam [26]
actor learning rate weight decay	0
actor learning rate scheduler	CosineAnnealingWarmupRestart [35]
actor learning rate cycle steps	100
critic optimizer	Adam
critic learning rate scheduler	CosineAnnealingWarmupRestart
critic scheduler warmup	10
critic learning rate cycle steps	100

Table 7: ReinFlow’s Hyperparameters in OpenAI Gym Locomotion Tasks

(a) Shared Hyperparameters Across OpenAI Gym Tasks

Parameter	Value
critic learning rate weight decay	1e-5
number of parallel environments	40
reward discount factor γ	0.99
action chunking size	4
condition stacking number	1
batch size	50k
maximum episode steps	1000
number of rollout steps	500
update epochs	5
number of training iterations	1000
number of denoising steps	4
clipping ratio ϵ	0.01
clip intermediate actions	True
target KL divergence	1.0
noise std upper bound hold for	35% of total iteration
noise std upper bound decay to	$0.3 \times \sigma_{\min} + 0.7 \times \sigma_{\max}$
entropy coefficient α	0.03
BC loss (W_2 regularization) coefficient β	0.00

(b) Task-Specific Hyperparameters in OpenAI Gym Environment

Parameter	Hopper-v2	Walker2d-v2	Ant-v0 Humanoid-v3
minimum noise std σ_{\min}	0.10	0.10	0.08
maximum noise std σ_{\max}	0.24	0.24	0.16
critic warmup iters	0	5	0
actor learning rate	$\cos(4.5e-5, 2.0e-5)$	$\cos(4.5e-4, 4.0e-4)$	$\cos(4.5e-5, 2.0e-5)$
critic learning rate	$\cos(6.5e-4, 3.0e-4)$	$\cos(4.0e-3, 4.0e-3)$	$\cos(6.5e-4, 3.0e-4)$

Table 8: ReinFlow’s Hyperparameters in Franka Kitchen State-input Manipulation Tasks

Parameter	Value
critic learning rate weight decay	1e-5
number of parallel environments	40
reward discount factor γ	0.99
action chunking size	4
condition stacking number	1
batch size	5600
maximum episode steps	280
number of rollout steps	200
update epochs	10
number of training iterations	301
number of denoising steps	4
clipping ratio ϵ	0.01
clip intermediate actions	True
minimum noise std σ_{\min}	0.05
maximum noise std σ_{\max}	0.12
noise std upper bound hold for	100% of total iteration
noise std upper bound decay to	σ_{\max}
entropy regularization coefficient α	0.00
BC loss (W_2 regularization) coefficient β	0.00

Table 9: ReinFlow’s Hyperparameters in Robomimic Visual Manipulation Tasks

(a) Shared Hyperparameters Across Robomimic Tasks

Parameter	Value
critic learning rate weight decay	0
number of parallel environments	50
reward discount factor γ	0.999
condition stacking number	1
pixel input shape	[3, 96, 96]
image augmentation	RandomShift (padding=4)
gradient accumulation steps	15
batch size	500
update epochs	10
clipping ratio ϵ	0.001
clip intermediate actions	True
target KL divergence	1e-2
noise std upper bound hold for	100% of total iteration
noise std upper bound decay to	σ_{\max}
BC loss (W_2 regularization) coefficient β	0.00

(b) Task-Specific Hyperparameters in Robomimic Environment

Parameter	PickPlaceCan	NutAssemblySquare	TwoArmTransport
minimum noise std σ_{\min}	0.08	0.08	0.05
maximum noise std σ_{\max}	0.14	0.14	0.10
number of denoising steps	1	1	4
entropy coefficient α	0.00	0.01	0.00
critic warmup iters	2	2	5
critic output layer bias	0.0	0.0	4.0
actor learning rate warmup	10	25	10
actor learning rate	$\cos(2.0e-5, 1.0e-5)$	$\cos(3.5e-6, 3.5e-6)$	$\cos(3.5e-6, 3.5e-6)$
critic learning rate	$\cos(6.5e-4, 3.0e-4)$	$\cos(4.5e-4, 3.0e-4)$	$\cos(3.2e-4, 3.0e-4)$
action chunking size	4	4	8
number of cameras	1	1	2
maximum episode steps	300	400	800
number of rollout steps	300	400	400
number of training iterations	150	300	200

G.2 Hyperparameters of DPPO

We strictly follow the hyperparameter setting of the official implementation of DPPO. Please refer to Section E.10 of [42] for details.

The only changes we make are incorporating seeds 509 and 2025 for furniture tasks and elongating the rollout steps from 70 to 200 (while we still keep the maximum episode length as 280 in the environment configuration). DPPO and ReinFlow exhibit higher variability in Franka kitchen tasks across random seeds and even different runs, so we adopt five random seeds. We also find that a longer sampling trajectory helps the DPPO agent discover optimal strategies. For this reason, DPPO achieves a higher task completion rate than that reported by DPPO’s original paper.

G.3 Hyperparameters of FQL

We list the hyperparameters adopted by FQL in Table 10. We set the number of offline pre-training steps such that the total sample consumption during the offline phase is no less than the pre-trained consumption of DPPO or ReinFlow in Gym (D4RL) and Franka Kitchen tasks.

As described in [38], the temperature coefficient, α_{FQL} , is the most important hyperparameter of FQL. We followed the instructions of the original paper and scanned α_{FQL} in $[0.03, 0.1, 0.3, 1, 3, 10]$ to obtain a proper value for the temperature in Hopper-v2. and adopted the same value for all state-input tasks.

Table 10: Hyperparameters for FQL in Gym and Franka Kitchen Tasks

(a) Shared Hyperparameters for FQL		
Parameter		Value
number of denoising steps of the base policy π_θ		4
number of steps for evaluation		500
number of evaluation episodes		10
reward discount factor γ		0.99
actor learning rate		$1e-4$
actor weight decay		0
actor learning rate cycle steps		1000
actor scheduler warmup		10
critic learning rate		$3e-4$
critic learning rate weight decay		0
critic scheduler warmup		10
batch size		256
target EMA rate		0.005
reward scale		1.0
buffer size		$1e6$
Behavior cloning coefficient		3.0
actor update repeat		1
online steps		569,936
(b) Task-Specific Hyperparameters in Robomimic Environment		
Parameter	Gym and Kitchen-complete-v0	Kitchen-mixed-v0 and Kitchen-partial-v0
offline steps	200,000	600,000